Clays and Clay Minerals, Vol. 67, No. 5:371–398, 2019

GEOLOGY, MINERALOGY, GEOCHEMISTRY, AND GENESIS OF BENTONITE DEPOSITS IN MIOCENE VOLCANO–SEDIMENTARY UNITS OF THE BALIKESIR REGION, WESTERN ANATOLIA, TURKEY

Selahattin Kadir[1] *, Tacit Külah[2], Hülya Erkoyun[1], George E. Christidis[3], and Raffi Arslanyan[1]

[1]Department of Geological Engineering, Eskişehir Osmangazi University, TR–26480 Eskişehir, Turkey
[2]Department of Geological Engineering, Kütahya Dumlupınar University, TR–43100 Kütahya, Turkey
[3]Department of Mineral Resources Engineering, Technical University of Crete, GR–73100 Chaniá, Greece

Abstract—The widespread Balıkesir bentonite deposits within the Miocene volcano-sedimentary units in western Anatolia have economic potential; they are important raw materials for the paper and bleaching industries in Turkey. No detailed geological, mineralogical, geochemical, or genesis characterizations of these bentonite deposits have been carried out to date. The present study was undertaken to close this gap. The mineralogical characteristics of the bentonites and their parent rocks were examined using polarized-light microscopy, X-ray powder diffractometry (XRD), scanning- and transmission-electron microscopies (SEM–EDX and TEM), and chemical (ICP–AES and –MS) methods. In the bentonite deposits, smectite is associated with smaller amounts of illite, chlorite, quartz, feldspar, dolomite, calcite, opal-CT, and amphibole. The smectite was identified by sharp basal reflections at 14.42–14.93 Å. Plagioclase and sanidine crystals in volcanic units are altered and sericitized. Biotite and hornblende are partly to completely Fe-(oxyhydr)oxidized and chloritized. Smectite flakes occur on altered feldspar and mica grains and devitrified volcanic glass fragments in association with or without calcite ± dolomite crystals. Increasing Al+Fe+Mg/Si ratios with increasing degree of alteration reveal that hydration of volcanogenic grains (feldspar, mica, hornblende, glass shard) favored precipitation of smectite with montmorillonite composition, with an average structural formula: $(Ca_{0.31}Na_{0.05}K_{0.08})(Al_{2.72}Fe_{0.17}Mg_{1.27}Ti_{0.011}Mn_{0.01})(Si_{7.94}Al_{0.06})O_{20}(OH)_4$. The concentration of Al_2O_3 and MgO and increase of LREE/HREE ratio, and a distinct, negative Eu anomaly show that smectite was probably formed as a result of the decomposition of volcanic feldspar, mica, amphibole, and volcanic glass. Association of carbonate rocks within the smectite-rich material and the absence of chlorite and detrital materials such as rock fragments in the bentonites suggest that the bentonite deposits formed authigenetically as 'primary bentonites' from volcanoclastic materials deposited in a calm lacustrine–palustrine environment during an early diagenetic process.

Keywords—Balıkesir · Bentonite · Genesis · Geochemistry · Mineralogy · Volcanic units · Turkey

INTRODUCTION

Smectite is commonly formed by weathering or by diagenetic or hydrothermal alteration of volcanic glass or minerals such as feldspars, micas, olivine, hornblende, and augite of volcanic and pyroclastic rocks and is the main constituent of bentonites (Grim & Güven 1978; Elliott 1993; Christidis et al. 1995; Christidis & Dunham 1997; Christidis & Scott 1997; Christidis 1998, 2001; Wulaningsih et al. 2013; Ghanem & Jarrar 2013; Motoki et al. 2015; Kadir et al. 2017). During alteration, the glass shards and igneous minerals react with meteoric water or hydrothermal fluids via a solid-solution mechanism, resulting in micro- and macro-scale physicochemical environmental conditions – characterized by local variations of Al, Mg, and Fe – and a pH in the range of 8 to 9 favor the precipitation of smectite (Huff et al. 1991; Ver Straeten 2004; Takagi et al. 2005; Środoń et al. 2006; Ray et al. 2011; Paz et al. 2012; Osborn et al. 2014; Ekinci Şans et al. 2015; Huff 2016). These microenvironmental geochemical variations may vary considerably yielding significant compositional variations of smectites (Christidis & Dunham 1997). These microenvironmental conditions may also favor precipitation of carbonates (dolomite, siderite), due to increase in Mg/Ca or Fe/Ca activity ratios and the consumption of Al during/following formation of smectite (Weaver & Beck 1977).

The Miocene volcano-sedimentary units are widespread in the tectonic Balıkesir basin in western Anatolia and were altered, resulting in the development of kaolinite, halloysite, alunite, and borate deposits with economic potential (Ece & Schroeder 2007; Ece et al. 2008, 2013). Although most of these deposits in western Anatolia developed under a tectonically controlled hydrothermal alteration process in the Miocene

* E-mail address of corresponding author: skadir_esogu@yahoo.com
DOI: 10.1007/s42860-019-00029-w

volcanic units, the absence of hydrothermal clues such as lateral and vertical mineralogical and geochemical zonation and sulfur and iron phases (Mutlu et al. 2005; Kadir & Akbulut 2009; Kadir & Kart 2009; Kadir et al. 2011) in the study area suggest that the genesis of Balıkesir bentonite is still open to debate.

The mineralogical and geochemical properties of Yeniköy and Bigadiç (Balıkesir) bentonites were studied by Kocabaş (2006) and Çoban (2014). Prior to this research, no detailed information was available concerning the mineralogical or geochemical characteristics and genesis of the bentonite deposits of the Miocene volcanic units in the Balıkesir area, which have economic potential as raw material for use in the paper and bleaching industries in Turkey. The aim of the present study was, therefore, to determine the mineralogy and geochemistry of the bentonite deposits and discuss their genetic relationship with volcano-sedimentary units. A further purpose was to compare bentonite deposits of the eastern Aegean Islands of Samos, Chios, and Thrace of the same age and geological environment (Ekinci Şans et al. 2015; Koutsopoulou et al. 2016). This comparison aimed to underline the main parameters which controlled the formation of these deposits and to interpret the differences observed between the various deposits of the broader area, taking into account the composition of the parent rocks.

GEOLOGICAL SETTING AND DEPOSITIONAL ENVIRONMENT

Geological Setting

Basement rocks of the area studied comprise Paleozoic–Mesozoic metamorphic rocks, Upper Cretaceous (Maastrichtian) Bornova Flysch, and Upper Cretaceous Yayla ophiolitic mélange (Fig. 1). Paleozoic-Mesozoic metamorphic rocks are composed of recrystallized limestones and marbles and are overlain tectonically by Upper Cretaceous (Maastrichtian) Bornova Flysch. The Bornova Flysch crops out at the southwestern side of the İzmir-Ankara-Erzincan Suture Zone (IAESZ) and consists of olistoliths and ophiolitic blocks bearing intensely sheared and folded detrital sediments (Konuk 1977; Akdeniz 1980; Erdoğan et al. 1990; Okay & Siyako 1993; Okay et al. 1996, 2001). The Bornova Flysch is overlain tectonically by the Upper Cretaceous Yayla ophiolitic mélange. The Yayla ophiolitic mélange is composed of serpentinite, basalt, gabbro, agglomerate, tuff, radiolarite-mudstone, sandstone, claystone, and recrystallized limestone and is overlain unconformably by Lower Miocene Kocaiskan volcanics. This unit is the first product of the Miocene volcanism in western Anatolia and is composed of andesitic lava and pyroclastic rocks. The unit is overlain unconformably by the Miocene Bigadiç volcano–sedimentary succession (BVSS). The BVSS is composed of volcanic (rhyolitic and dacitic Sındırgı volcanics, Gölcük Basalt, trachyandesitic dikes of the Kayırlar Volcanics, and basalts and andesites of the Şahinkaya Volcanics) and lacustrine sediments intercalated with volcano-sedimentary units (Erkül et al. 2005a). Lacustrine sediments of the BVSS comprise mudstone, claystone, marl, evaporites, and silicified limestone intercalated with tuff and tuffite. This unit has been described as the Soma Formation by Akyürek & Akdeniz (1989) and Pehlivan et al. (2007). These tectonically deformed and folded sediments are also intercalated locally with bituminous shale and coal levels (Akyürek & Akdeniz 1989). All the aforementioned formations are overlain unconformably by Quaternary alluvium (Fig. 2).

Lithology

The lithologies which have been distinguished within the bentonite-bearing Miocene Bigadiç volcano–sedimentary succession in the Balıkesir region are described below.

Mudstone

This mudstone facies is characterized by different thicknesses (10–50 cm) of mudstone layers in the bentonite deposits. The mudstones are light brown in color. They contain desiccation cracks, relict plant rootlets, and Mn oxide stains (Fig. 3a).

Marl

This marl facies is white to cream in color, thin bedded (10–50 cm), and contains desiccation cracks filled by relict plant rootlets and Mn oxide stains (Fig. 3b).

Limestone and dolomitic limestones

This facies is characterized mainly by dolomitic limestones, white to cream in color, medium to thick bedded (1–3 m), is fractured, Mn oxide stained, and contains silica bands and local occurrences of argillaceous limestone (Fig. 3c,d).

Claystone

This facies is characterized by white, beige, and locally light brown, 10–100 cm thick, smectite-rich clays in the bentonite deposits. The claystones contain recent desiccation cracks, relict plant rootlets, and Mn oxide stains as fracture in-fills (Fig. 3e,f).

Tuff

This facies is friable, locally massive and thin bedded (30 cm–5 m). It is composed mainly of ash and locally epiclastic rock fragments and volcanic materials, such as pumice, volcaniclastic grains, and devitrified glass shards. It is pink, white, or grayish-white in color. The composition of the tuff ranges from rhyolitic to andesitic and the tuffaceous units show intense argillization (Fig. 3g,h).

General Features of Bentonite Deposits

Bentonites and volcano-sedimentary samples of the Balıkesir region were collected from four recently mined bentonite deposits within the BVSS. The bentonite deposits are described below by name, beginning with the bentonites in the

https://doi.org/10.1007/s42860-019-00029-w Published online by Cambridge University Press

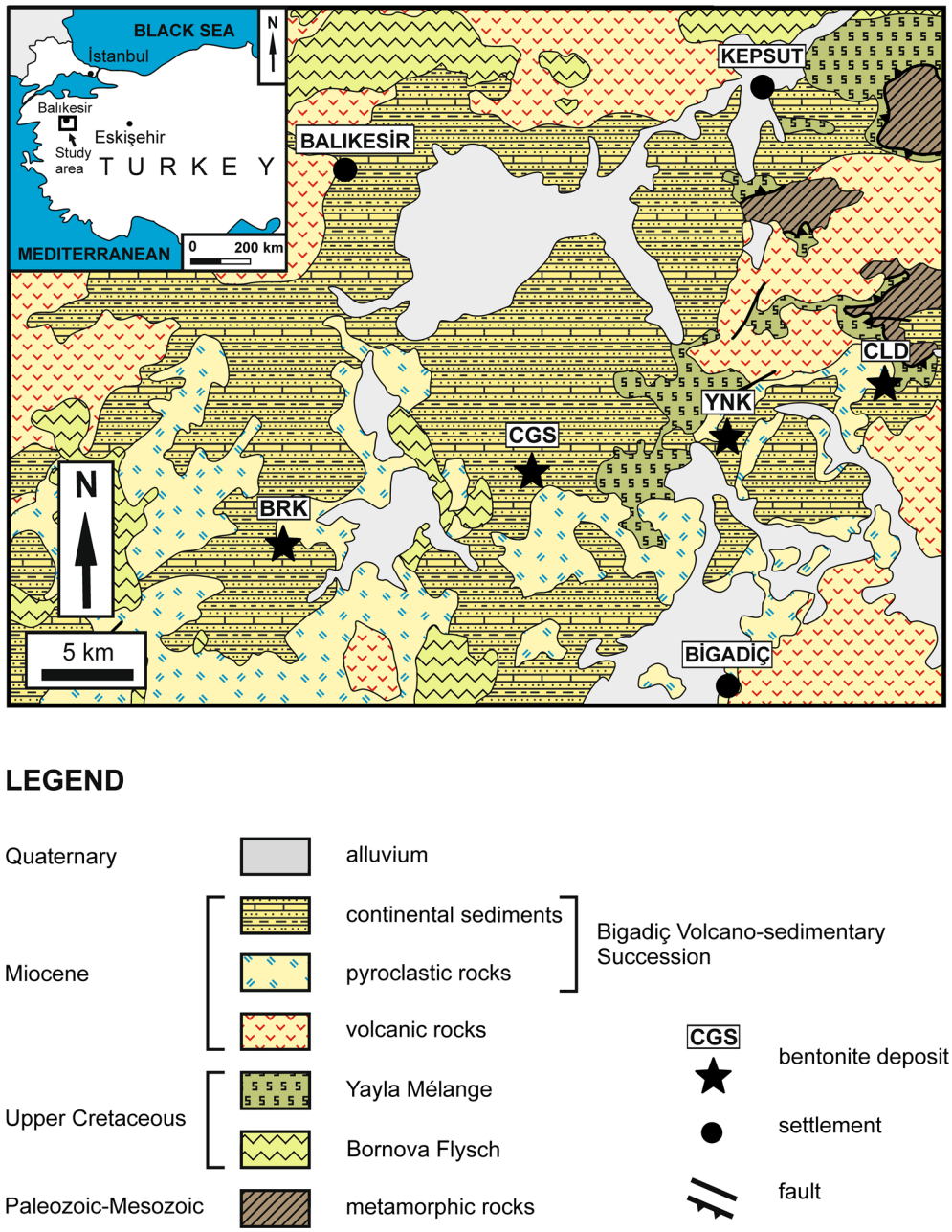

Fig. 1 Geological map of the Balıkesir area (modified from MTA 2002)

northeast of the study area and progressing southward (Figs. 3 and 4).

Çaldere deposit (CLD)

This bentonite deposit lies within the sediments of the BVSS as a N–S trending syncline. This deposit contains cream to white colored bentonite with alternating beige bentonite layers rich in Fe oxide. The bentonite continues upward with beige bentonite and is overlain by silicified, dolomitic limestone layers of the BVSS. The total thickness of this Ca-bentonite is ~30 m (Fig. 3g,h). The Çaldere bentonite deposit is currently being mined and ~12,000 tons of bentonite is produced annually for the paper and bleaching industries in Turkey (Bakır et al. 2012).

Yeniköy deposit (YNK)

The Yeniköy bentonite deposit also lies within the sediments of the BVSS as a N–S trending syncline. A beige-colored bentonite overlies a grayish-white-colored basal tuff of the BVSS (Fig. 3i). This bentonite has recent desiccation

https://doi.org/10.1007/s42860-019-00029-w Published online by Cambridge University Press

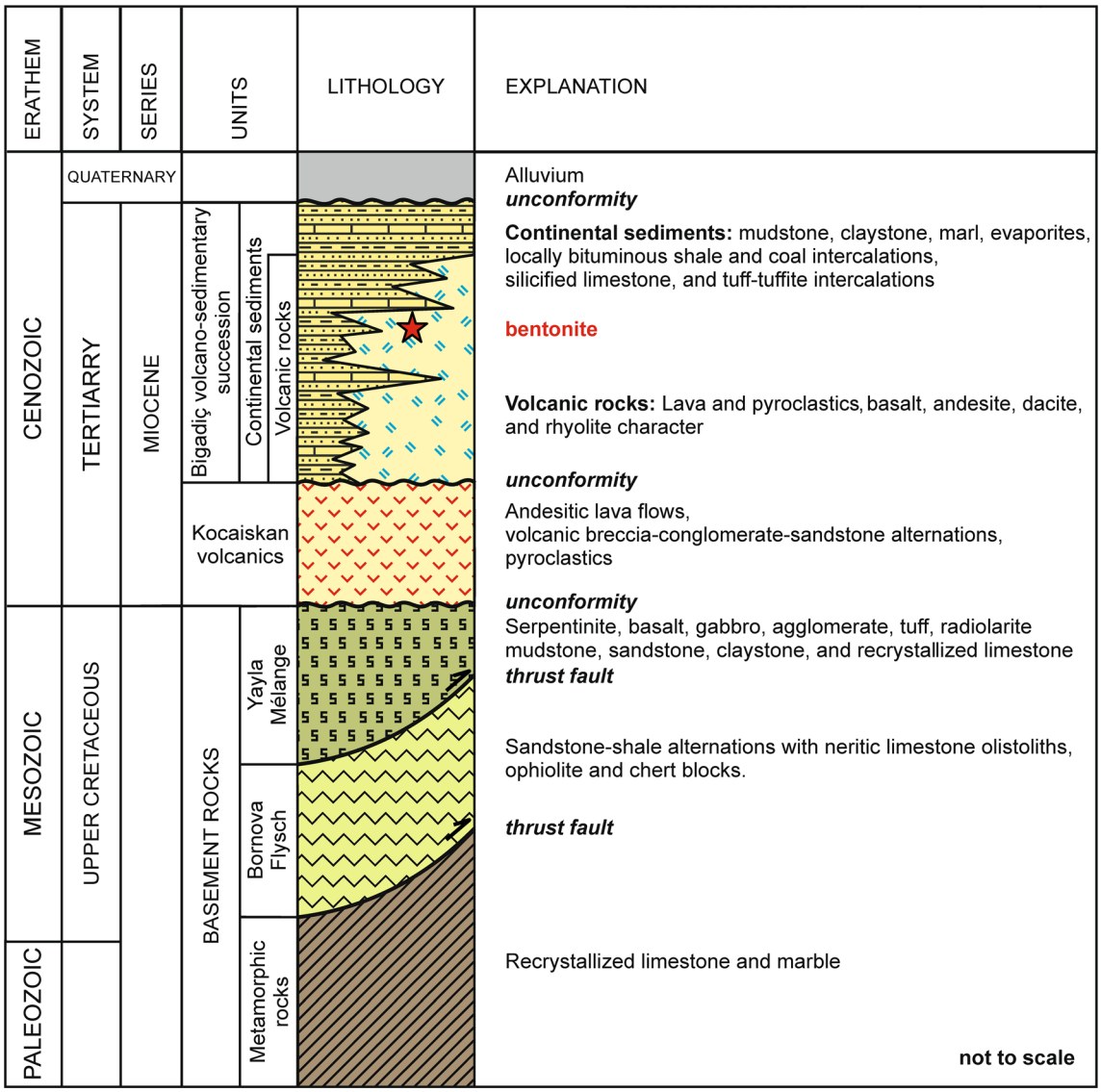

Fig. 2 Stratigraphic section of the Balıkesir area (modified from Akyürek & Akdeniz 1989; Erkül et al. 2005a; Pehlivan et al. 2007). Stratigraphic symbols are as defined in Fig. 1

cracks, plant rootlets, and, locally, Fe oxide stains. The total thickness of this Ca-bentonite is ~10 m, and upward is succeeded by light brown, thin-bedded argillaceous tuff and white, argillaceous, nodular limestone layers. This deposit was discovered earlier and was mined for the paper and bleaching industries in Turkey (Bakır et al. 2012).

Çağış deposit (CGS)

The Çağış bentonite deposit lies within intensely folded and faulted sediments of the BVSS (Fig. 3j). This deposit starts at the lower contact as a white bentonite and exhibits conchoidal fracture, plastic and recently formed desiccation cracks. This bentonite also has silica and opal intercalations of varying thickness of 1–5 m. The Çağış deposit is covered by cream- to beige-colored, silicified limestone, marl, and mudstone alternations which are 10–15 m thick. The total thickness of the bentonite in this deposit is ~25 m. This deposit contains an appreciable tonnage of both Na- and Ca-bentonite and is currently being mined for the paper and bleaching industries in Turkey, but the reserve quantity has not been calculated (Bakır et al. 2012).

Bereketli deposit (BRK)

In this deposit, light brown, thin-bedded mudstones of the BVSS underlie the beige, conchoidal-fractured, and locally ferromagnesian mineral fragments such as amphibole-and biotite-bearing bentonite (Fig. 3k). This bentonite incorporates argillaceous tuff intercalations of various

https://doi.org/10.1007/s42860-019-00029-w Published online by Cambridge University Press

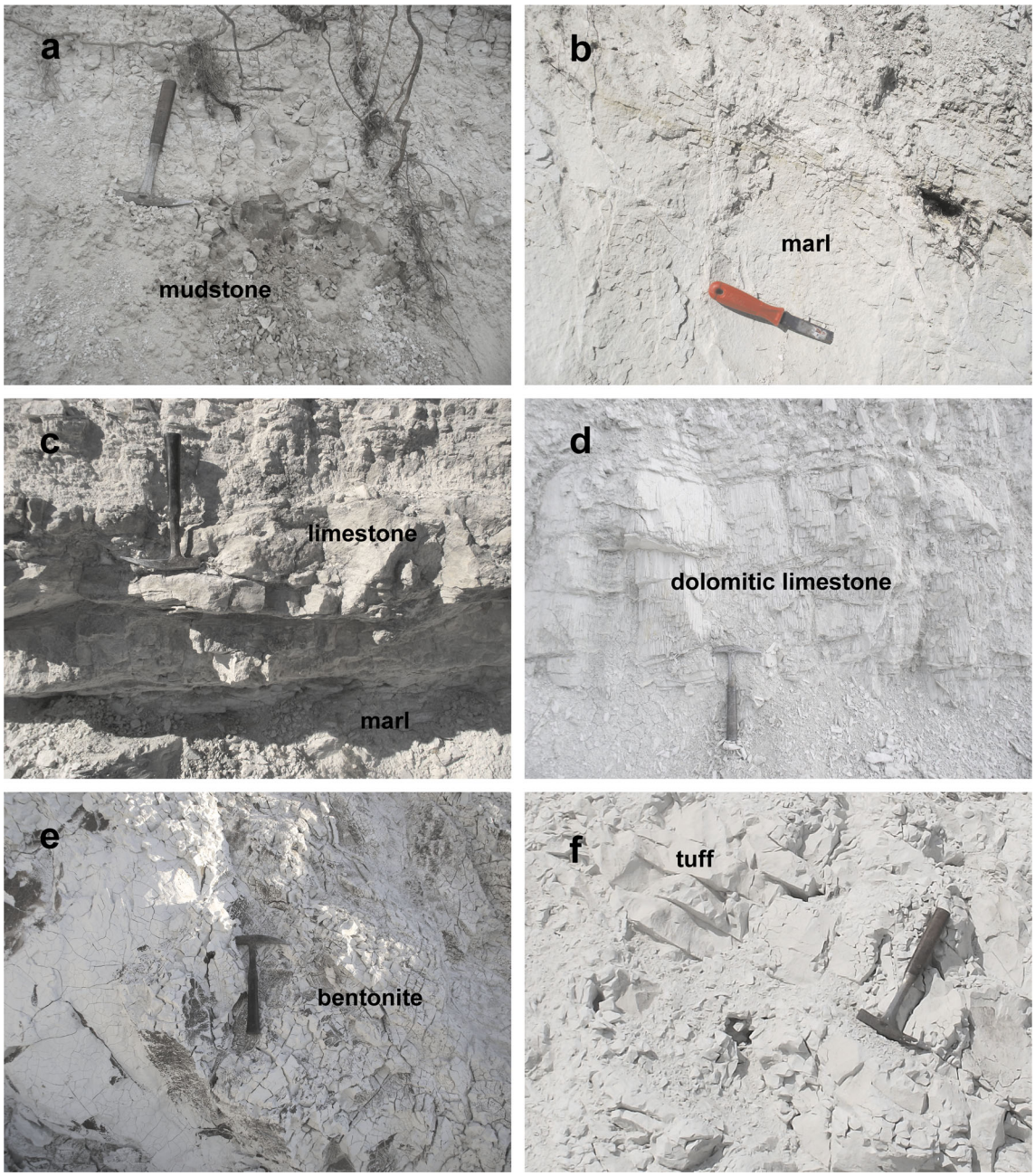

Fig. 3 Field photographs of the Balıkesir bentonite deposits. **(a)** Mudstone in the Bereketli bentonite deposit; **(b)** marl layers in the Yeniköy bentonite deposit; **(c,d)** alternation of carbonate and marl units in the Çağış bentonite deposit; **(e)** close-up view of bentonite in the Çağış bentonite deposit; **(f)** tuffaceous units intercalating the Çağış bentonite deposit; **(g,h)** general view of the Çaldere bentonite deposit; **(i)** general view of the Yeniköy bentonite deposit hosted by a tuffaceous unit and overlained by carbonate; **(j)** general view of the Çağış bentonite deposit overlain by carbonate; **(k)** Bereketli bentonite deposit intercalating tuffaceous units; and **(l)** enlarged view of k

thickness between 5 and 50 cm (Fig. 3l). The total thickness of bentonite in this deposit is ~5. This bentonite is covered by ~6 m of cream- and pink-colored tuff and tuffite layers enclosing silt-to-sand sized pumice and rock fragments of the BVSS. This deposit was previously discovered and mined to supply paper and bleaching industries in Turkey (Bakır et al. 2012).

MATERIALS AND METHODS

Field work was carried out using the existing 1/500,000 scale geological map of the Balıkesir region (Fig. 1; MTA 2002) to determine the distribution of bentonite deposits and related volcano-sedimentary units in the area studied. Up to 500 g of bentonite was collected from each of the various stratigraphic sections (Fig. 4). Optical microscope studies

https://doi.org/10.1007/s42860-019-00029-w Published online by Cambridge University Press

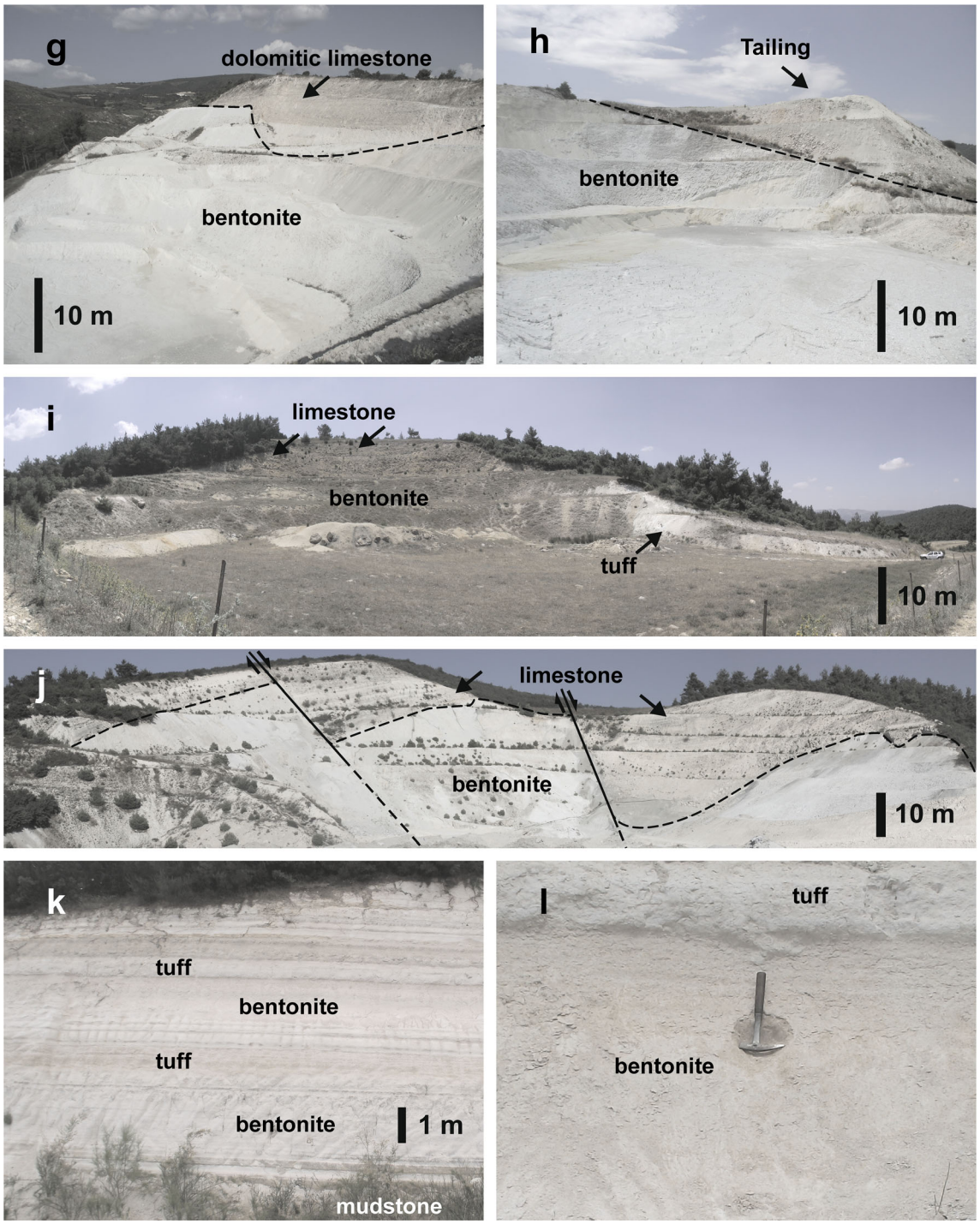

Fig. 3 (continued)

using a Nikon-LV 100 Pol (Nikon Corporation, Tokyo, Japan) were carried out in thin section of fresh volcanic rock samples. Selected samples that represent various degrees of alteration were manually crushed and powdered using a tungsten carbide pulverizer for X-ray diffraction (XRD) and geochemical analyses.

Separation of the clay fraction followed the removal of Fe(III) oxide cements, carbonate cements, and organic matter (Kunze & Dixon 1986). The treated samples were sieved to <2 mm and 100 g of the <2 mm fraction was mixed with deionized water and disaggregated using a 'Stir-Pak' (Cole-Parmer, Vernon Hills, Illinois, USA)

https://doi.org/10.1007/s42860-019-00029-w Published online by Cambridge University Press

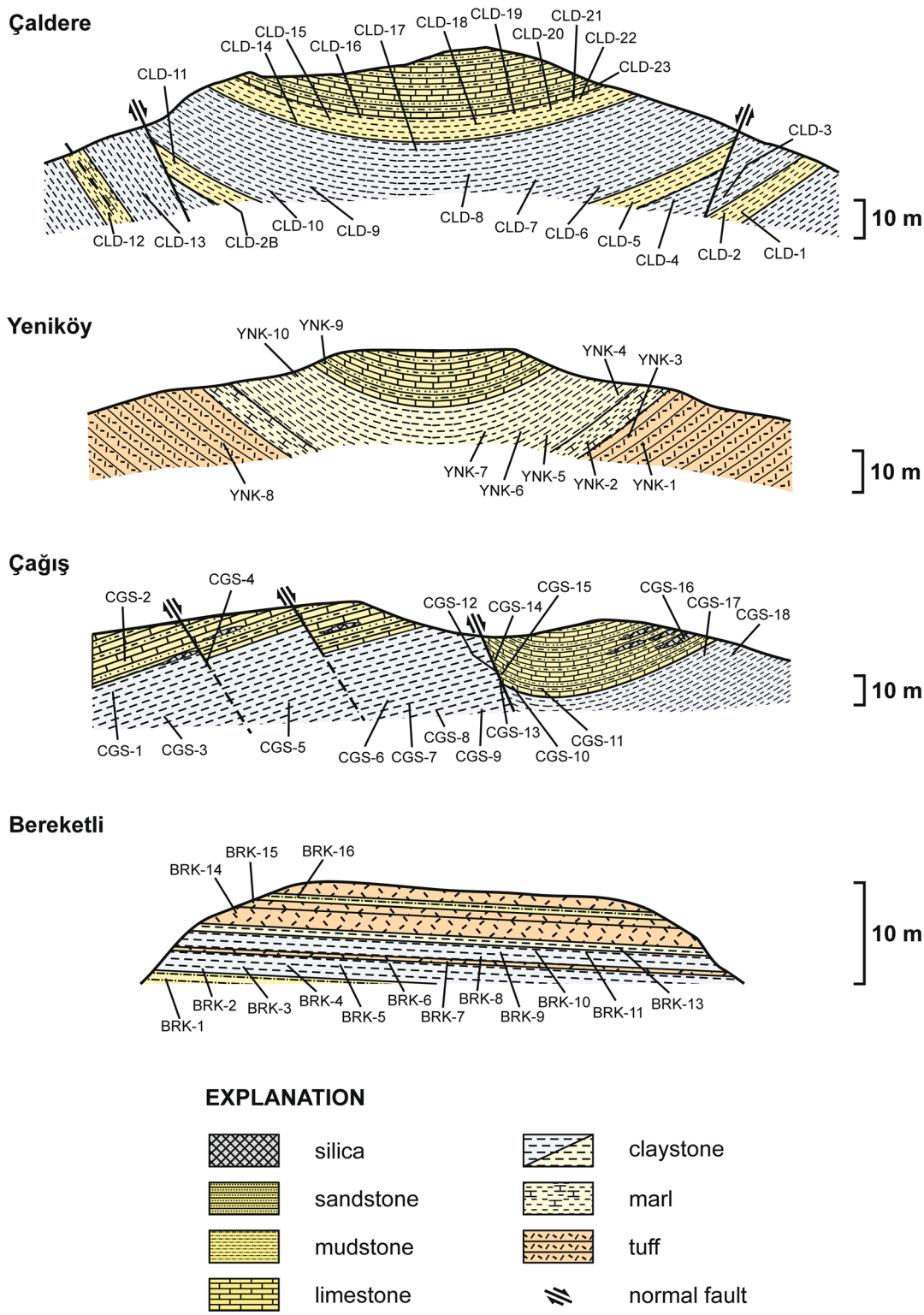

Fig. 4 Sketch of the Balıkesir bentonite deposits

mixer head and mixer controller. The <2 μm fractions were separated from the silt (2–50 μm) by repeated siphoning of the dispersed material. The clay fraction (<2 μm) was separated by sedimentation of the suspension after 24 h of dispersion in distilled water and removal of the upper 5 cm, followed by centrifugation for 10 min at

https://doi.org/10.1007/s42860-019-00029-w Published online by Cambridge University Press

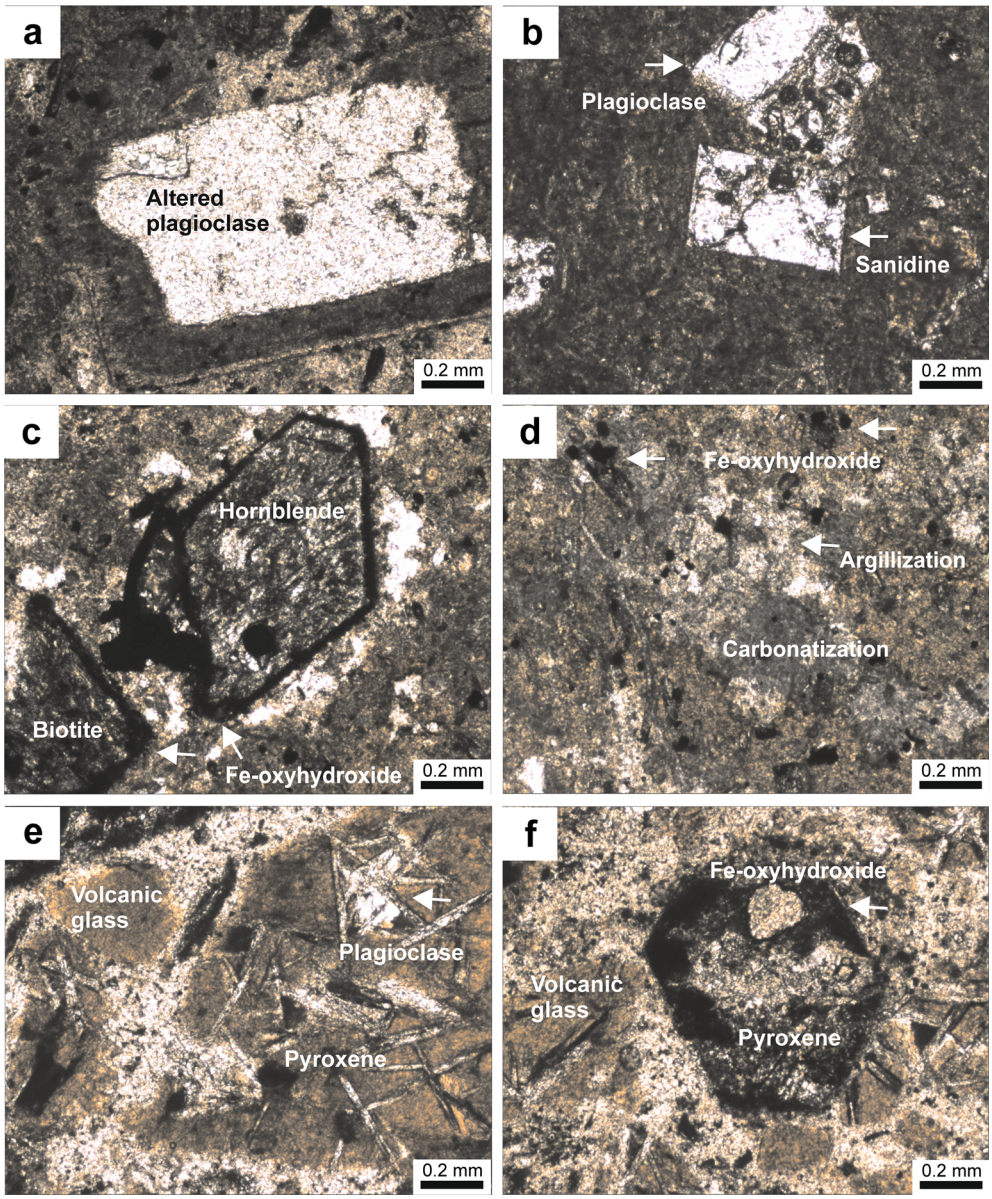

Fig. 5 Photomicrographs of: **(a–c)** altered feldspar, hornblende and biotite in tuff, plane-polarized light (BRK-14, CLD-24); **(d)** carbonatization, argillization, and Fe-(oxyhydr)oxidation in rhyolitic tuff, plane-polarized light (HBP-16); **(e)** pyroxene crystals between plagioclase in spilitic basalt, showing intersertal texture, plane-polarized light (HBP-13); and **(f)** a pyroxene crystal in spilitic basalt, plane-polarized light (HBP-13)

2451×*g* (4000 rpm) using a Hettich 32A centrifuge (Andreas Hettich GmbH and Co. KG, Tuttlingen, Germany).

The mineralogical characteristics of the samples were determined using powder XRD with a Rigaku D / Max – 2200 with an Ultia PC (Rigaku Corporation, Tokyo, Japan). The XRD analyses were performed using CuKα radiation with a scanning speed of 1°2θ/min and a tube voltage and current of 40 kV and 30 mA, respectively. Bulk mineralogy was determined using random powder mounts. Several oriented mounts were prepared, from each clay fraction separated as noted above, by dropping a small amount of clay suspension onto a glass slide and drying in air. One oriented mount was solvated using ethylene glycol (EG) vapor at 60°C for 2 h to identify smectites. Other oriented mounts were heated at 300 and 550°C for 2 h to identify chlorite and kaolinite.

Quantitative analysis of the samples was performed on random powder samples (side loading mounting) emplaced in Al-holders, by the Rietveld method using the BGMN computer program (*Autoquan*© software package version 2.8), on a Bruker D8 Advance Diffractometer equipped with a Lynx Eye strip silicon detector, and using Ni-filtered CuKα radiation (35 kV, 35 mA) at the Technical University

https://doi.org/10.1007/s42860-019-00029-w Published online by Cambridge University Press

of Crete (Greece). Data were collected in the range 3–70°2θ with a step size of 0.02°2θ and counting time of 1 s per strip step (total time 63.6 s per step).

Representative smectite-dominated bulk samples were prepared for scanning electron microscopy-energy dispersive X-ray analysis (SEM-EDX) using double-sided tape to adhere the fresh, broken surface of each sample to an Al sample holder and by coating the samples thinly with fine Au particles (350 Å) using a Giko IB-3 ion coater (Giko Engineering Co. Ltd., Nagoya, Japan). The analyses were performed at Middle East Technical University (Ankara, Turkey) using a QUANTA 400*F* Field Emission SEM instrument (Thermo Fisher Scientific, Hillsboro, Oregon, USA). Transmission electron microscopy (TEM) studies were carried out at the Bilkent University (Ankara, Turkey) using an FEI Tecnai F30™ (FEI/Thermo Fisher Scientific, Hillsboro, Oregon, USA) instrument. The clay particles for TEM analysis were dispersed in an ultrasonic ethanol bath for ~30 min, and one drop of each clay suspension was placed on a carbon-coated copper grid and dried at room temperature.

The chemical analyses of 13 bentonite, six argillaceous carbonate/calcareous claystone, and four tuff samples were performed at the Bureau Veritas Mineral Laboratories (Vancouver, Canada) using a PerkinElmer Elan 9000 (PerkinElmer Inc., Waltham, Massachusetts, USA) inductively coupled plasma-atomic emission spectrometer (ICP-ES), a mass spectrometer (ICP-MS), and a Spectro (Spectro Analytical Instruments Inc., Mahwah, New Jersey, USA) XLAB-2000 PED X-ray fluorescence spectrometer (PEDXRF), which was calibrated using USGS inter-laboratory standards. The detection limits for the analyses were between 0.01 and 0.1 wt.% for major elements, 0.1 and 5 ppm for trace elements, and 0.01 and 0.5 ppm for REE (rare earth elements).

The degree of chemical index of weathering (CIW) of bentonite, argillaceous carbonate/calcareous claystone, and tuff whole-rock samples was calculated using Eq. 1 (Harnois 1988):

$$\mathrm{CIW} = [\mathrm{Al_2O_3}/(\mathrm{Al_2O_3} + \mathrm{CaO^*} + \mathrm{Na_2O})] \times 100 \quad (1)$$

where CaO* is the amount of CaO incorporated in the silicate fraction.

The structural formula of smectite was determined in the <2 μm clay fractions of samples with the largest smectite content. The smectite-rich clay fractions were separated using the method described above. The amount of SiO_2 polymorphs in the clay fraction was corrected for impurities that were not removed and not detected by XRD. The structural formula of smectite was calculated based on $O_{20}(OH)_4$.

Fresh tuffaceous units that represent the parent rock of the bentonite were used for mass-gain and mass-loss calculations. Mass gains and losses have been calculated and estimated using the *EASYGRESGRANT* program (Eq. 2) (López-Moro 2012) and from isocon diagram plots of the geochemical analyses (Grant 1986, 2005):

$$C_i^A = \left(M^O/M^A\right) C_i^O \quad (2)$$

where C_i is the concentration of component i, ^{O} indicates the fresh rock, and ^{A} indicates the altered rock. The M^O and M^A values are the equilibrium masses (as wt.% or ppm) of the fresh and altered rocks, respectively.

The C_i^A/C_i^O ratios were plotted to obtain the slopes of the isocon graphic lines from the fresh and the altered rock analytical data using Eq. 3:

$$\Delta C_i/C_i^O = \left(M^A/M^O\right)\left(C_i^A/C_i^O\right) - 1 \quad (3)$$

where ΔC_i is the gain or loss of mass. MnO was assumed to be immobile based on clusters of slopes that were close to 1.00.

If a constant mass is assumed (Eq. 4),

$$\Delta C_i^A/C_i^O = \left(C_i^A/C_i^O\right) - 1 \quad (4)$$

Thus, sample compositions that plot above the isocon line indicate a mass gain during the alteration process and samples that plot below this line represent a mass loss during alteration.

RESULTS

Petrography

The parent rock of bentonite in the Balıkesir region is composed of rhyolitic and andesitic tuffs and spilite (basalt). Rhyolitic and andesitic tuff show porphyritic texture, are composed of plagioclase (albite-andesine), and are partly to completely altered, locally showing sericitization and zonation (Fig. 5a,b). Sanidine crystals show Carlsbad twining and are partly altered (Fig. 5b). Biotite and hornblende crystals are partly to completely altered to Fe-(oxyhydr)oxides and are locally chloritized (Fig. 5c). The groundmasses of rhyolitic and andesitic tuffs consist of plagioclase microlites with argillitic and carbonate alteration, and Fe-(oxyhydr)oxidation products (Fig. 5d). Spilitic basalt is composed of pyroxene crystals and plagioclase microlite in a volcanic groundmass, showing intersertal texture (Fig. 5e,f).

XRD Determinations

The quantitative analyses with Rietveld refinement and representative XRD traces of the bentonite and their parent rock bulk samples are given in Table 1 and Fig. 6, respectively. Smectite is abundant, sometimes associated with minor illite and accessory chlorite and kaolinite in the bentonites and altered volcanic units. The smectite content varies between broad limits, from a few wt.% in argillaceous carbonates and calcareous claystones to >90 wt.% in bentonites (Table 1). These minerals are accompanied by quartz, K-feldspar, plagioclase, dolomite, calcite, and opal-CT. Accessory amphibole, talc, serpentine, and pyrophyllite are present in the Çağış deposit. The abundance of calcite and dolomite increases in the upper level of the Çaldere and Çağış bentonite deposits.

Smectite was identified by a sharp reflection at 14.42–14.93 Å that shifted to 16.09–16.97 Å after EG solvation and collapsed to 9.53–9.90 Å and 9.43–9.86 Å after heating at 300 and 550°C for 2 h, respectively (Fig. 6).

https://doi.org/10.1007/s42860-019-00029-w Published online by Cambridge University Press

Table 1 Mineralogical variations (wt.%) in the Balıkesir bentonite deposits from analysis of XRD patterns for claystone samples

Sample	Rock type	Sme	Ilt	Kln	Chl	Kfs	Pl	Qz	Opl	Cal	Dol	Hbl	Srp	Tlc	Php
Çaldere															
CLD-2B	Bentonite	57.7				2.3	2.0	0.7	37.3						
CLD-4	Bentonite	90.2				3.2	5.5	1.1							
CLD-11	Bentonite	90.1				5.5		1.5		2.9					
CLD-12	Bentonite	25.7								74.3					
CLD-14	Bentonite	42.6				2.1	1.1	0.4			53.8				
CLD-16	Bentonite	39.1				3.5		0.9	35.1		21.4				
CLD-18	Calcareous claystone	23.5	1.8			7.5	6.1	1.6		59.5					
CLD-19	Bentonite	57.7				3.6		1.0	20.0		17.7				
CLD-20	Calcareous claystone	4.0							2.8	93.2					
CLD-23	Argillaceous carbonate	1.0	0.7						0.5	0.8	97.0				
Yeniköy															
YNK-2	Calcareous claystone	9.2	2.5			4.2		0.8	6.4	76.9					
YNK-4	Bentonite	11.5					1.8			86.7					
YNK-5	Bentonite	82.5				3.4	5.9	0.5	7.7						
YNK-6	Bentonite	91.4				4.9		1.5		2.2					
YNK-10	Bentonite	76.8				11.2	4.4	2.8			2.8				
Çağış															
CGS-4	Bentonite	19.4	17.7	4.1	5.0	8.9	14.5	16.5				6.9	1.7	5.3	
CGS-7	Bentonite	93.6				5.1		1.3							
CGS-11	Calcareous claystone	14.5	2			3.8	22.6	1.8		49.5		3.2			2.6
CGS-12	Bentonite	3	2.8	1.2	2	1.1	1.7	2.2		84.8		0.5		0.7	
CGS-13	Bentonite	94.3				4.6		1.1							
CGS-14	Argillaceous carbonate						0.5	0.5	30.2	0.5	68.3				
CGS-18	Bentonite	89.8				5.5	3.8	0.9							
Bereketli															
BRK-1	Bentonite	20.3	24.5	5.8		11.4	16.5	12		8		1.5			
BRK-3	Bentonite	69.5	6.1			8.5	9.4	4.0	1.0	1.5					
BRK-6	Bentonite	76.0	6.9			4.2	9.1	2.1		1.7					
BRK-10	Bentonite	60.0				13.5	16.2	8.6		1.7					

Abbreviations: Sme: smectite; Ilt: illite; Kln: kaolinite; Chl: chlorite; Kfs: K-feldspar; Pl: plagioclase; Qz: quartz; Opl: Opal-CT; Cal: calcite; Dol: dolomite; Hbl: hornblende; Srp: serpentine; Tlc: talc, Php: phillipsite (mineral-name abbreviations after Whitney & Evans 2010)

SEM–EDX and TEM Analyses

The SEM images indicated that volcanic materials such as feldspar, mica, and glass shards are highly altered and yielded the cement material in these units (Fig. 7a–d). Smectite flakes developed in microfractures and dissolution voids of altered feldspar and devitrified glass shard and at the edge of platy mica via dissolution and precipitation. The sizes of flaky smectite mostly increase from the fracture centers toward their margins (Fig. 7e–g). Locally, the volcanic unit encloses abundant euhedral dolomite crystals associated with smectite crystals and a network of calcified filaments (Fig. 7h–j).

The TEM images confirmed the flaky morphology of smectite (Fig. 8a,b). The diameter of the smectite flakes varies between 0.1 and 0.3 μm.

Chemical Analyses

Chemical analyses of bentonite units are characterized by moderate concentrations of SiO_2 (average 55.10 wt.%), Al_2O_3 (average 14.77 wt.%), MgO (average 4.40 wt.%), Fe_2O_3 (average 2.30 wt.%), and CaO (average 2.30 wt.%) and small concentrations of Na_2O (average 0.49 wt.%) and K_2O (average 1.48 wt.%). Loss on ignition (LOI) is considerable, reflecting the presence of smectite (average 18.68 wt.%). Concentrations of trace elements such as Ba (average 295 ppm), Rb (average 103 ppm), Sr (average 126 ppm), and Zr (average 114 ppm) decrease in bentonite relative to the parent tuff (Table 2). In addition, argillaceous carbonate/calcareous claystone samples have smaller concentrations of SiO_2 (average 36.3 wt.%), Al_2O_3 (average 5.96 wt.%), Fe_2O_3 (average 1.33 wt.%), Na_2O (average 0.28 wt.%), and K_2O (average 0.68 wt.%),

https://doi.org/10.1007/s42860-019-00029-w Published online by Cambridge University Press

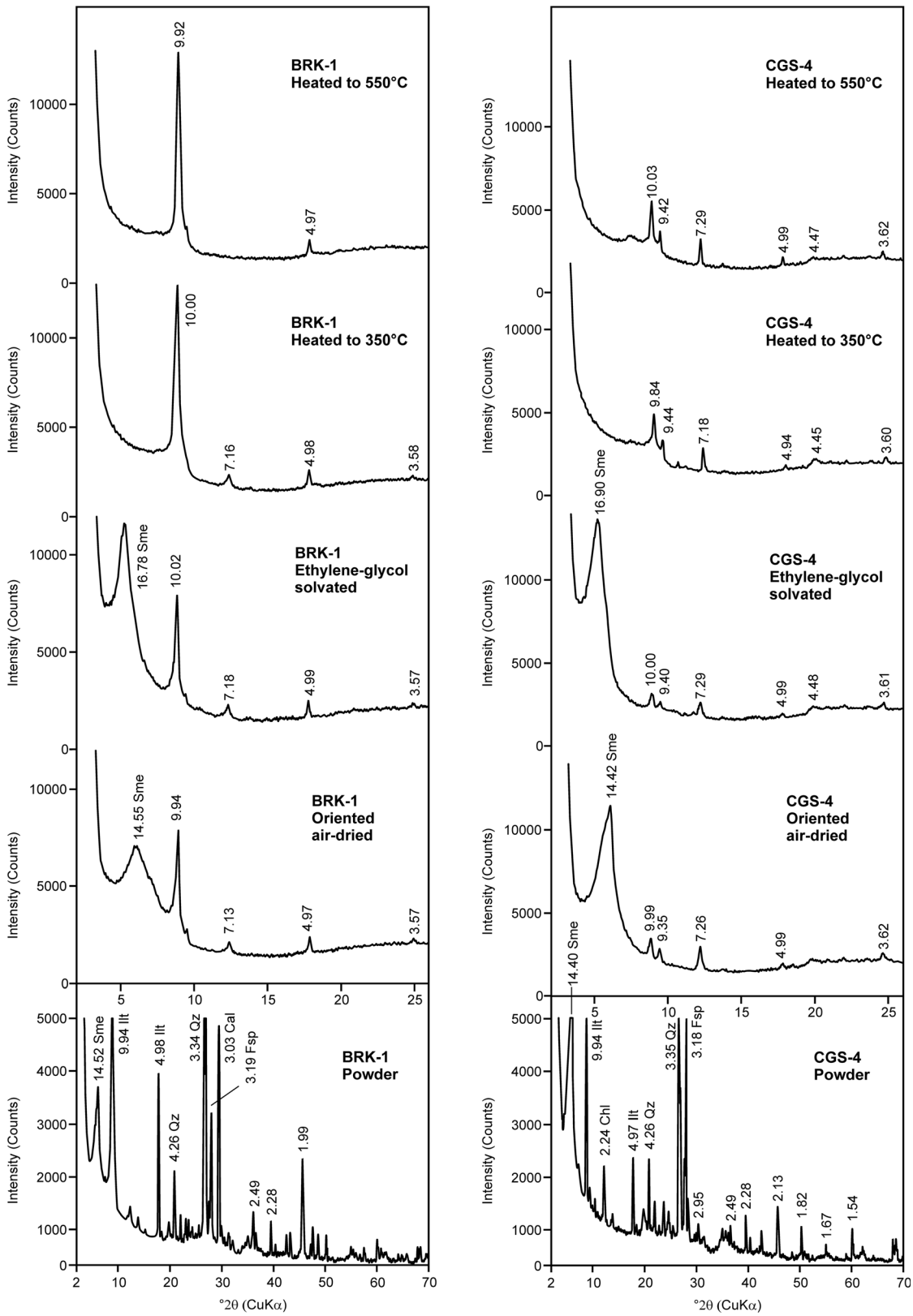

Fig. 6 XRD patterns for Balıkesir bentonite samples. Sme: smectite; Ilt: illite Chl: chlorite, Fsp: feldspar, Qz: quartz, Opl: Opal-CT, Cal: calcite, Dol: dolomite (mineral-name abbreviations after Whitney & Evans 2010)

https://doi.org/10.1007/s42860-019-00029-w Published online by Cambridge University Press

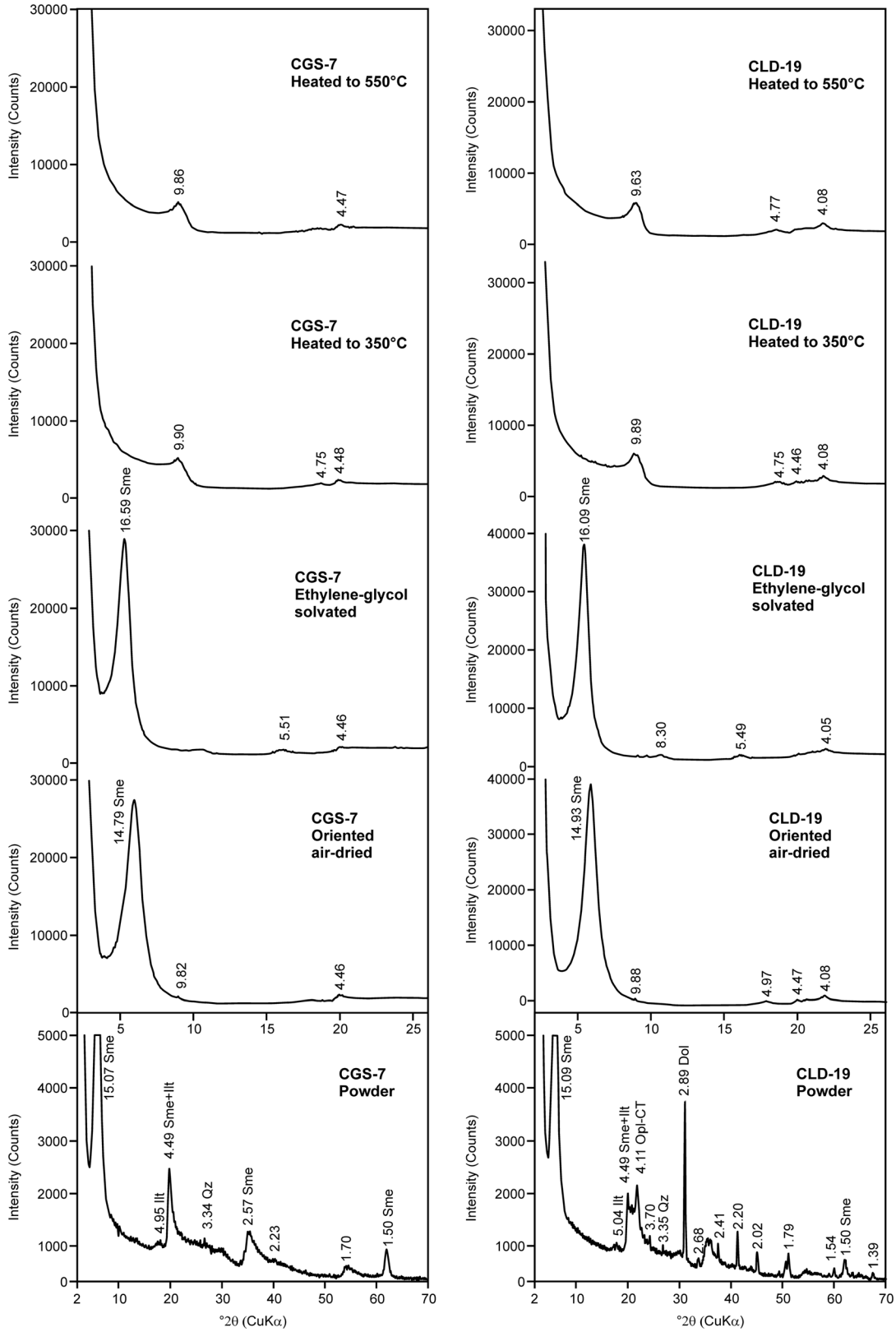

Fig. 6 (continued)

https://doi.org/10.1007/s42860-019-00029-w Published online by Cambridge University Press

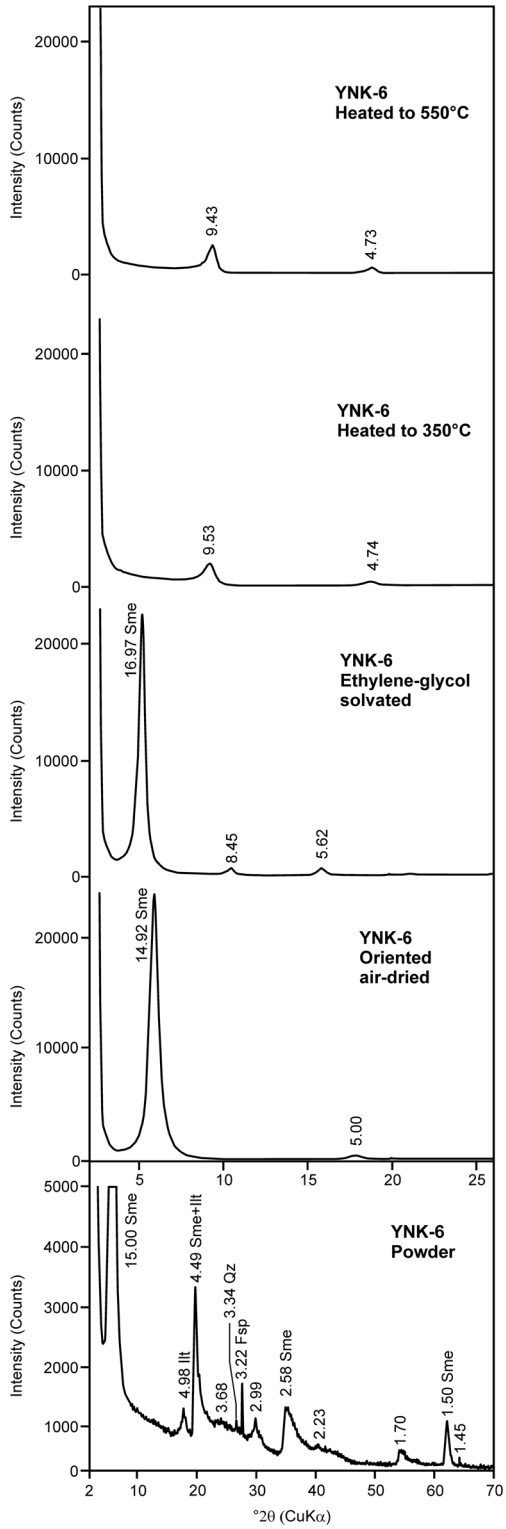

Fig. 6 (continued)

compared to the bentonites, and more MgO (average 7.54 wt.%), CaO (average 19.8 wt.%), and LOI (average 27.47 wt.%) compared to the bentonites. These units are characterized by the presence of Ba (average 154 ppm), Rb (average 34 ppm), Sr (average 2574 ppm), and Zr (average 50 ppm). The observed compositional differences between the bentonite and the argillaceous carbonate/calcareous claystone samples reflect the relative abundance of carbonates admixed with the volcanic material.

The tuffaceous units representing a parent rock of the bentonite are characterized by greater abundances of SiO_2 (average 63.87 wt.%), Al_2O_3 (average 15.57 wt.%), Fe_2O_3 (average 2.83 wt.%), Na_2O (average 1.78 wt.%), and K_2O (average 3.61 wt.%), and smaller abundances of MgO (average 2.44 wt.%), CaO (average 1.78 wt.%), and LOI (average 6.9 wt.%) compared to the bentonite samples (Table 2).

The mass gains and losses based on the plots of the geochemical analyses on isocon diagrams (Grant 1986, 2005) showed that SiO_2, Fe_2O_3, Na_2O, K_2O, Ba, Sr, Rb, V, and Zr were released, while MgO, CaO, Cr, Nb, Th, and Y were enriched during alteration based on the best-fit isocon slope (m = 1.00) (Table 3; Fig. 9a–f). MnO shows an immobile nature based on clusters of slopes close to 1.00.

The REE of bentonite, argillaceous carbonate/calcareous claystone, and tuff were normalized to chondrite values and primitive mantle (Sun & McDonough 1989; Fig. 10a,b). Light rare earth elements (LREE) are enhanced compared to middle rare earth elements (MREE) and heavy rare earth elements (HREE), with negative Eu anomalies ($Eu/Eu^* = 0.30–0.93$). According to mass-balance calculations the LREE and Eu were depleted during alteration of the tuffs to bentonite, whereas HREE were enriched (Table 2). These trends are the opposite of those observed during the formation of the Kimolian bentonites from alteration of acidic volcanic rocks (Christidis 1998). The carbonate/calcareous claystones have small REE abundances (Fig. 10a,b) due to the influence of dilution by carbonates (e.g. Table 1).

The CIW values for bentonite, argillaceous carbonate/calcareous claystone, and tuff are 79.59%, 28.84%, and 73.76%, respectively, suggesting the presence of a wide-ranging alteration process in the volcanic units (Table 2). The CIW of bentonite is higher than that of the parent tuff, whereas those of the carbonate/calcareous claystones are considerably lower. The low CIW values of the carbonate/calcareous claystones reflect the presence of carbonates (abundance of CaO and MgO).

When plotted on a discrimination diagram (Winchester & Floyd 1977) the parent rocks of the different bentonites have rhyolitic and andesitic-trachyandesitic affinities (Fig. 11). Projection on the discrimination diagram of Hastie et al. (2007) shows that the bentonites have high-K and shoshonitic affinities based on the crossplot of Co vs. Th (Fig. 12). The bentonites from the eastern Aegean and Thrace display similar

https://doi.org/10.1007/s42860-019-00029-w Published online by Cambridge University Press

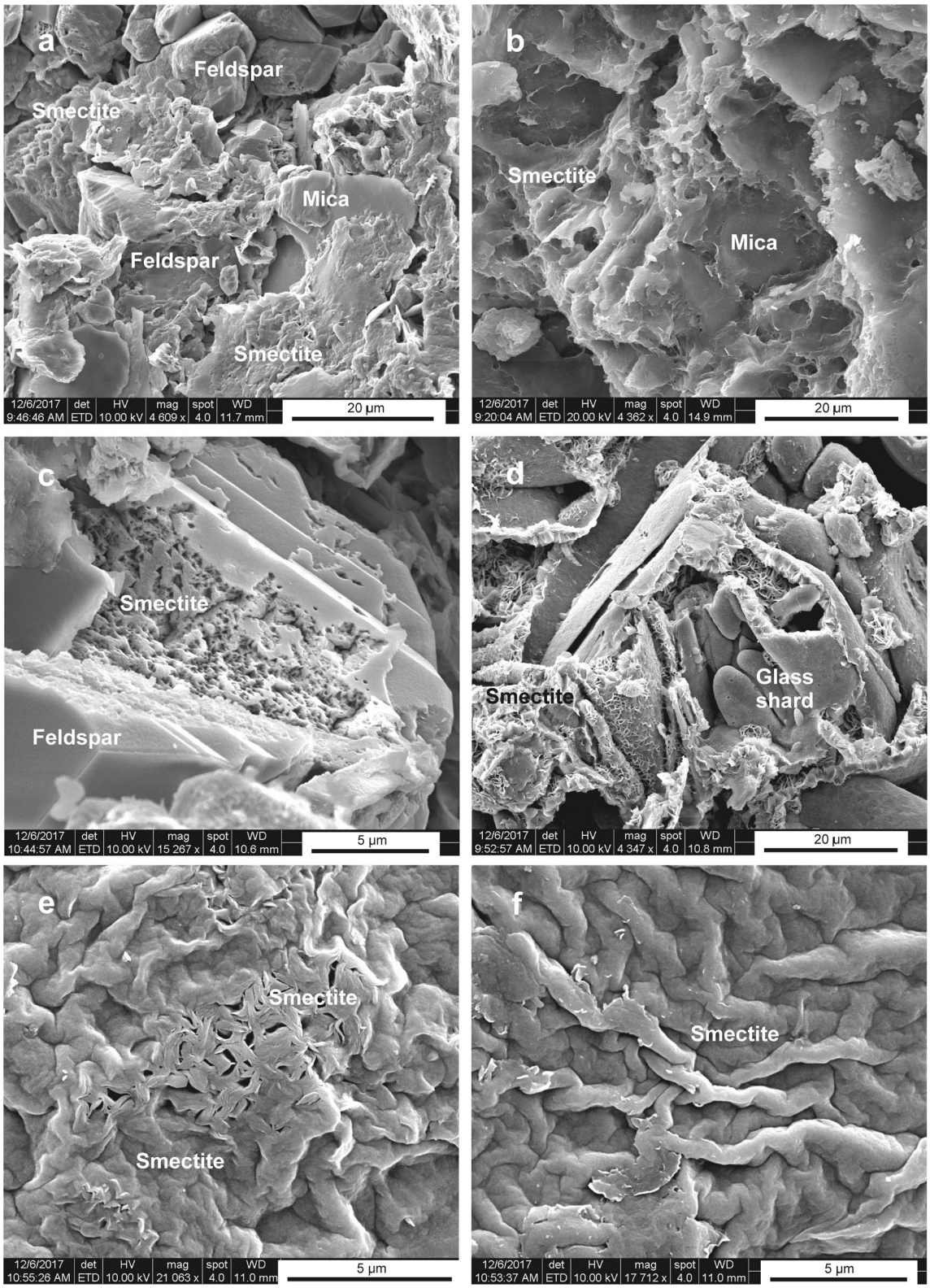

Fig. 7 SEM images of: **(a,b)** flaky smectite matrix between resorbed feldspar and mica-abundant volcanic materials (CGS-12, CGS-4); **(c)** relic of altered feldspar enclosing flaky smectite (BRK-1); **(d)** devitrified volcanic glass edging smectite (BRK-6); **(e)** the formation of smectite in microfractures of previously formed smectite (CLD-11); **(f)** close-up view of a dense smectite crystal (CLD-11); **(g)** smectite flakes in pore (CLD-4); **(h)** the formation of smectite as cement between dolomite crystals (CLD-16); **(i)** rhombohedral dolomite crystal (CLD-16); and **(j)** dolomite crystals covered by microorganisms (CLD-16)

https://doi.org/10.1007/s42860-019-00029-w Published online by Cambridge University Press

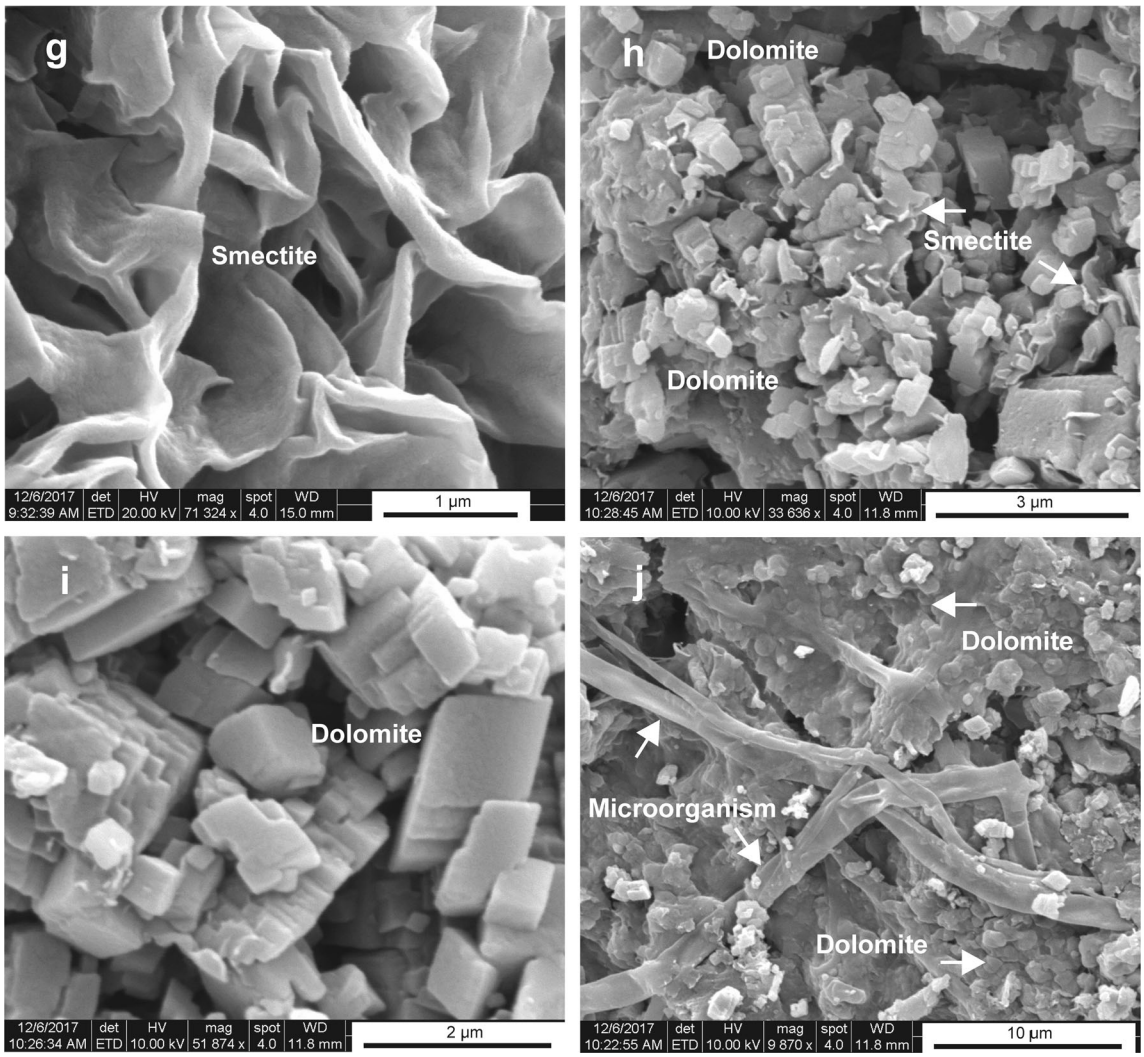

Fig. 7 (continued)

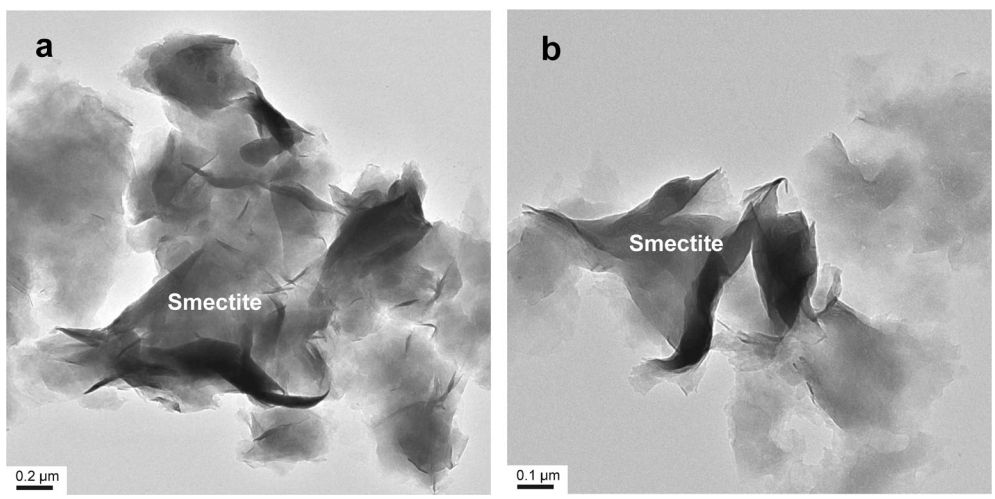

Fig. 8 TEM images of: (**a**,**b**) smectite crystals (BRK-6, CLD-4)

https://doi.org/10.1007/s42860-019-00029-w Published online by Cambridge University Press

Table 2 Major oxide (wt.%), minor element (wt.%), and trace element (ppm) contents of the bentonite, argillaceous carbonate/calcareous claystone and volcanic parent rock samples in the study area (see Table 1 for the mineralogical compositions of the samples)

	Bentonite								
Major oxides (wt. %)	CLD-4	CLD-9	CLD-11	YNK-10	CGS-4	CGS-7	CGS-8	CGS-13	CGS-17
SiO_2	52.54	58.75	50.70	57.51	59.38	51.79	64.23	51.45	50.75
Al_2O_3	15.23	13.57	15.01	17.62	14.09	14.04	12.56	14.81	13.90
Fe_2O_3	1.49	1.59	1.69	6.02	4.40	1.55	1.22	1.52	1.42
MgO	5.85	3.78	6.60	1.39	4.45	6.95	2.44	5.64	6.25
CaO	1.33	2.22	2.00	0.02	2.74	1.29	1.40	1.97	1.77
Na_2O	0.11	0.18	0.05	0.04	1.65	0.06	0.77	0.05	0.04
K_2O	0.24	0.53	0.32	2.91	1.74	0.24	4.04	0.19	0.17
TiO_2	0.07	0.09	0.10	0.73	0.58	0.09	0.06	0.09	0.08
P_2O_5	<0.01	<0.01	0.02	0.06	0.10	0.01	0.01	0.01	0.02
MnO	<0.01	0.04	0.02	0.01	0.09	<0.01	0.04	0.04	0.12
Cr_2O_3	<0.002	<0.002	<0.002	<0.002	0.028	<0.002	<0.002	<0.002	<0.002
LOI	23.0	19.0	23.3	13.5	10.5	23.8	13.1	24.1	25.3
Total	99.86	99.81	99.84	99.84	99.82	99.84	99.89	99.86	99.82
CIW	85.63	97.43	80.32	99.42	64.79	85.14	76.87	80.33	80.95
Trace elements (ppm)									
Ni	2.3	1.9	4.2	9.3	79	4.9	4.4	10.4	5.1
Sc	3	3	4	18	10	4	3	4	4
Ba	58	304	101	555	462	74	105	71	143
Be	7	4	2	<1	2	5	5	3	7
Co	0.4	1.4	0.9	18.2	17.9	0.4	0.2	0.4	0.9
Cs	6.4	325.9	20.2	6.1	23.7	5.2	21.3	2.9	2.7
Ga	16.2	13.5	15.1	19.9	13.0	14.0	12.4	15.7	14.9
Hf	4.7	4.3	4.8	5.5	4.2	4.1	4.0	4.5	4.5
Nb	22.9	12.5	21.0	14.2	22.7	18.7	18.3	20.3	20.3
Rb	10.2	124.7	25.2	135.9	88.8	12.1	298.1	8.0	7.3
Sn	6	4	6	3	2	6	5	6	6
Sr	87.0	263.9	82.1	151.7	259.1	132.5	56.2	89.7	131.1
Ta	2.1	1.4	1.9	1.3	0.9	2.0	1.8	1.9	1.9
Th	39.6	34.1	39.9	47.7	15.2	37.6	34.1	36.7	37.1
U	2.0	1.7	0.7	11.9	1.9	0.7	6.5	0.3	1.5
V	<8	20	<8	107	67	19	<8	13	64
W	<0.5	<0.5	<0.5	1.3	2.3	<0.5	2.9	1.2	3.2
Zr	112.8	119.2	114.1	201.5	158.2	104.6	90.5	108.3	107.6
Y	9.2	29.6	28.0	23.2	30.2	9.4	28.5	16.7	37.9

Table 2 (continued)

La	14.8	58.6	30.9	62.3	60.1	34.9	22.6	20.1	24.2
Ce	30.7	126.1	56.3	111.2	62.8	28.0	47.0	44.3	108.8
Pr	3.38	11.01	6.14	11.35	10.73	6.47	5.00	4.61	5.61
Nd	12.1	37.3	21.7	39.5	37.3	21.2	17.6	15.5	21.5
Sm	2.66	6.69	4.66	6.91	6.99	3.72	4.42	3.62	5.64
Eu	0.14	0.65	0.27	1.49	0.90	0.21	0.19	0.21	0.29
Gd	2.02	5.47	4.45	4.87	5.69	2.46	4.33	3.09	5.61
Tb	0.34	0.84	0.75	0.69	0.87	0.35	0.76	0.53	1.03
Dy	2.01	4.99	4.62	4.14	4.85	1.84	4.69	3.17	6.42
Ho	0.37	1.00	0.92	0.87	0.96	0.30	1.00	0.65	1.32
Er	1.27	3.05	2.75	2.51	2.86	0.94	2.91	1.79	4.04
Tm	0.26	0.44	0.42	0.36	0.42	0.12	0.44	0.29	0.62
Yb	2.50	2.82	2.83	2.45	2.80	0.91	3.08	1.90	4.17
Lu	0.46	0.47	0.42	0.40	0.44	0.15	0.47	0.31	0.62
TOT/C	<0.02	0.03	0.30	0.02	0.04	<0.02	0.02	<0.02	<0.02
TOT/S	<0.02	<0.02	<0.02	4.87	<0.02	<0.02	<0.02	<0.02	<0.02
Mo	<0.1	<0.1	<0.1	3.8	0.2	<0.1	0.1	<0.1	0.5
Cu	1.0	1.8	0.8	89.0	14.9	1.9	0.6	1.3	1.8
Pb	48.9	25.0	30.9	50.9	53.2	27.0	18.4	39.7	78.6
Zn	36	10	17	35	43	31	14	30	30
As	2.2	71.9	50.7	10.3	11.7	7.6	9.8	6.1	20.4
Cd	<0.1	<0.1	<0.1	<0.1	<0.1	<0.1	<0.1	<0.1	<0.1
Sb	0.8	1.2	1.0	0.1	1.3	0.9	0.5	1.1	1.5
Bi	0.5	0.1	0.7	0.2	1.1	0.2	0.3	0.5	1.0
Ag	<0.1	<0.1	<0.1	<0.1	<0.1	<0.1	<0.1	0.9	<0.1
Au (ppb)	0.9	<0.5	1.2	<0.5	1.0	0.9	0.6	<0.5	<0.5
Hg	<0.01	<0.01	0.01	0.11	0.19	0.01	<0.01	<0.01	<0.01
Tl	<0.1	0.9	<0.1	1.0	1.1	0.2	<0.1	1.4	2.9
Se	<0.5	<0.5	0.6	6.2	<0.5	<0.5	<0.5	<0.5	<0.5
ΣREE	82.1	289.0	165.1	272.3	227.9	111.0	143.0	116.8	228.4
ΣLREE	60.9	233.0	115.0	224.4	170.9	90.6	92.2	84.5	160.1
ΣMREE	7.5	19.6	15.7	19.0	20.3	8.9	15.4	11.3	20.3
ΣHREE	4.5	6.8	6.4	5.7	6.5	2.1	6.9	4.3	9.5
Eu/Eu*	0.16	0.30	0.17	0.71	0.40	0.18	0.12	0.18	0.15

	Bentonite					Argillaceous carbonate/calcareous claystone			
Major oxides (wt. %)	CGS-18	BRK-1	BRK-6	BRK-10	avg.	CLD-16	CLD-19	CLD-23	CGS-12
SiO_2	52.02	47.96	54.57	64.68	55.10	60.54	51.97	26.89	23.49
Al_2O_3	15.20	16.11	15.75	14.06	14.77	8.32	10.16	0.27	7.43
Fe_2O_3	1.48	5.23	1.25	1.04	2.30	0.91	1.09	0.10	3.74
MgO	5.53	2.47	4.13	1.68	4.40	5.43	7.07	13.73	3.95
CaO	1.85	9.01	2.62	1.63	2.30	4.53	5.97	25.05	30.29
Na_2O	0.09	1.52	0.44	1.36	0.49	0.03	0.03	0.03	0.41
K_2O	0.20	3.86	0.86	3.95	1.48	0.16	0.16	<0.01	1.36

Table 2 (continued)

TiO_2	0.08	0.57	0.14	0.11	0.21	0.05	0.06	0.01	0.23
P_2O_5	<0.01	0.16	0.02	0.02	0.04	0.01	<0.01	0.02	0.05
MnO	0.04	0.06	0.19	0.09	0.06	0.02	0.02	<0.01	0.02
Cr_2O_3	<0.002	0.012	0.003	0.006	0.005	<0.002	<0.002	<0.002	0.034
LOI	23.4	12.7	19.9	11.3	18.68	19.9	23.3	32.2	28.8
Total	99.85	99.83	99.88	99.92	99.85	99.88	99.85	98.32	99.89
CIW	81.42	54.96	74.28	73.20	79.59	46.44	48.18	-	11.70
Ni	2.9	34.3	8.3	7.6	13.43	2.0	2.2	2.4	116.0
Sc	4	12	5	4	6.00	2	2	<1	8
Ba	76	1419	272	194	294.92	67	50	181	254
Be	6	1	3	7	4.08	2	2	<1	<1
Co	0.3	13.1	4.4	2.5	4.69	<0.2	0.3	0.6	12.8
Cs	4.1	56.7	7.2	10.0	37.88	11.6	7.6	0.9	13.8
Ga	15.8	21.1	17.1	19.6	16.02	8.2	9.9	<0.5	7.8
Hf	4.8	3.6	3.8	2.9	4.28	2.8	3.1	<0.1	1.0
Nb	20.4	15.1	21.8	19.7	19.07	12.6	13.3	<0.1	6.2
Rb	11.8	299.1	92.1	229.8	103.32	7.9	7.7	0.4	59.6
Sn	6	6	3	3	4.77	3	4	<1	1
Sr	126.3	134.5	71.8	56.3	126.32	113.6	144.1	12371.4	94.4
Ta	1.9	1.1	2.2	2.0	1.72	1.1	1.4	<0.1	0.2
Th	38.6	16.7	27.9	22.8	32.92	22.6	26.8	0.4	3.3
U	1.1	2.6	1.3	7.2	3.03	1.9	1.6	1.2	0.6
V	9	91	17	12	34.08	<8	<8	<8	65
W	1.1	3.9	5.8	3.2	2.07	0.5	0.6	<0.5	0.9
Zr	113.3	122.5	74.0	60.6	114.40	64.5	75.7	4.2	36.9
Y	11.5	50.5	26.7	21.4	24.83	12.2	8.0	0.4	7.7
La	24.4	38.5	11.7	8.5	31.66	21.1	14.8	0.9	15.1
Ce	29.9	81.2	24.5	15.9	58.98	42.8	31.2	1.4	11.6
Pr	5.00	8.70	2.91	2.10	6.39	4.77	3.14	0.16	2.62
Nd	16.5	32.4	10.9	7.9	22.42	16.7	10.9	0.6	9.4
Sm	3.49	7.01	3.13	2.38	4.72	3.57	2.09	0.07	1.86
Eu	0.18	1.16	0.52	0.39	0.51	0.18	0.14	0.03	0.27
Gd	2.60	6.66	3.67	2.72	4.13	2.71	1.69	0.11	1.63
Tb	0.39	1.14	0.67	0.51	0.68	0.45	0.27	0.01	0.25
Dy	2.21	7.28	4.29	3.08	4.12	2.64	1.52	0.06	1.44
Ho	0.42	1.49	0.86	0.71	0.84	0.48	0.29	<0.02	0.29
Er	1.17	4.35	2.68	2.18	2.50	1.43	0.88	0.05	0.79
Tm	0.19	0.63	0.41	0.33	0.38	0.22	0.15	<0.01	0.11
Yb	1.33	4.12	2.90	2.25	2.62	1.51	1.10	<0.05	0.71
Lu	0.21	0.63	0.43	0.38	0.41	0.24	0.19	<0.01	0.12
TOT/C	<0.02	1.73	<0.02	<0.02	0.18	1.47	1.95	6.82	6.69
TOT/S	<0.02	0.02	<0.02	<0.02	0.39	<0.02	<0.02	<0.02	<0.02
Mo	<0.1	0.1	0.3	0.4	0.46	<0.1	<0.1	1.3	<0.1
Cu	0.9	22.2	2.0	2.3	10.81	1.3	0.9	0.7	12.2
Pb	38.0	22.9	45.6	13.1	37.86	24.5	14.6	1.2	5.2

Table 2 (continued)

Zn	23	56	13	9	26.69	19	13	<1	50
As	2.5	47.3	5.2	1.4	19.01	13.9	6.6	22.1	1.9
Cd	<0.1	0.2	0.1	<0.1	0.11	<0.1	<0.1	<0.1	<0.1
Sb	1.2	0.9	0.4	0.3	0.86	0.5	0.3	0.8	0.3
Bi	0.4	0.5	1.2	0.4	0.55	0.2	0.5	<0.1	<0.1
Ag	<0.1	<0.1	<0.1	<0.1	0.16	<0.1	<0.1	<0.1	<0.1
Au (ppb)	1.8	5.4	<0.5	1.1	1.18	1.2	<0.5	5.2	<0.5
Hg	0.01	<0.01	0.04	<0.01	0.03	<0.01	<0.01	0.01	0.01
Tl	3.0	0.9	0.3	0.1	0.93	<0.1	<0.1	0.2	0.7
Se	<0.5	<0.5	<0.5	<0.5	0.95	<0.5	<0.5	<0.5	<0.5
ΣREE	99.5	245.7	96.2	70.7	165.21	111.0	76.3	<3.9	53.8
ΣLREE	75.8	160.8	50.0	34.4	119.43	85.4	60.0	3.1	38.7
ΣMREE	9.3	24.7	13.1	9.8	14.99	10.0	6.0	<0.3	5.7
ΣHREE	2.9	9.7	6.4	5.1	5.91	3.4	2.3	<0.12	1.7
Eu/Eu*	0.16	0.49	0.46	0.45	0.30	0.16	0.21	1.3	0.45
	Argillaceous carbonate/calcareous claystone			Tuff					
Major oxides (wt. %)	CGS-14	BRK-13	avg.	CLD-24	BRK-7	BRK-14	BRK-15	avg.	
SiO_2	16.29	38.67	36.31	56.07	69.55	62.18	67.66	63.87	
Al_2O_3	1.44	8.12	5.96	16.31	16.40	14.47	15.11	15.57	
Fe_2O_3	0.39	1.75	1.33	3.38	1.27	4.90	1.78	2.83	
MgO	13.58	1.50	7.54	6.11	0.89	1.95	0.82	2.44	
CaO	29.29	23.66	19.8	3.39	0.07	4.39	0.45	2.10	
Na_2O	0.06	1.11	0.28	3.35	0.04	2.31	1.42	1.78	
K_2O	0.37	2.01	0.68	3.69	3.85	3.05	3.84	3.61	
TiO_2	0.05	0.24	0.11	0.42	0.61	0.55	0.54	0.53	
P_2O_5	0.04	0.06	0.03	0.14	0.05	0.17	0.04	0.10	
MnO	0.01	0.06	0.02	0.04	0.02	0.17	<0.01	<0.06	
Cr_2O_3	<0.002	0.013	0.009	<0.002	<0.002	0.007	<0.002	<0.003	
LOI	37.9	22.7	27.47	6.7	7.1	5.6	8.1	6.9	
Total	99.46	99.91	99.55	99.78	99.86	99.86	99.90	99.85	
CIW	2.60	15.30	28.84	58.21	98.76	55.16	82.91	73.76	
Trace elements (ppm)									
Ni	2.8	30.3	25.95	1.4	1.5	9.1	1.6	3.4	
Sc	<1	5	3.17	5	12	9	8	8.5	
Ba	158	214	154	1417	216	760	1140	883	
Be	<1	2	1.5	2	2	<1	4	2.25	
Co	0.6	4.6	3.18	4.1	0.3	12.0	0.5	4.2	
Cs	3.2	21.1	9.7	10.7	15.5	1.5	4.2	8.0	
Ga	<0.5	10.2	6.18	15.9	18.1	13.4	14.0	15.4	
Hf	0.8	2.9	1.78	5.3	4.8	4.0	4.5	4.7	
Nb	1.5	11.1	7.47	12.0	11.5	10.5	12.1	11.5	
Rb	13.7	114.5	33.97	98.6	170.0	90.0	133.9	123.1	
Sn	<1	2	2	<1	2	1	2	<1.5	

Table 2 (continued)

Sr	2570.1	150.1	2574	382.6	102.9	376.3	208.7	267.6
Ta	0.1	0.7	0.6	0.9	1.1	1.0	1.2	1.1
Th	2.8	10.7	11.1	19.2	25.8	26.0	24.8	24.0
U	3.1	3.5	1.98	4.3	6.7	7.8	8.1	6.7
V	10	26	20.83	38	87	105	81	77.8
W	0.9	1.5	0.82	1.7	2.7	2.5	2.0	2.2
Zr	32.3	88.1	50.28	212.7	161.4	143.1	167.2	171.1
Y	3.0	29.9	10.2	15.2	11.4	18.4	12.2	14.3
La	4.5	24.2	13.43	43.4	52.5	42.6	33.8	43.1
Ce	7.7	27.2	20.32	73.8	86.1	73.3	57.0	72.6
Pr	0.86	4.88	2.74	7.45	7.81	7.71	6.00	7.24
Nd	3.3	18.3	9.87	24.9	25.7	26.8	21.5	24.7
Sm	0.53	3.98	2.02	3.93	3.27	4.54	3.79	3.88
Eu	0.11	0.66	0.23	0.90	0.74	1.10	0.85	0.90
Gd	0.59	4.41	1.86	3.03	2.00	3.94	2.95	2.98
Tb	0.09	0.72	0.3	0.45	0.28	0.56	0.39	0.42
Dy	0.51	4.68	1.81	2.54	1.76	3.11	2.24	2.41
Ho	0.12	1.01	0.37	0.53	0.40	0.59	0.46	0.50
Er	0.31	2.94	1.07	1.63	1.27	1.84	1.34	1.52
Tm	0.05	0.43	0.16	0.24	0.19	0.27	0.21	0.23
Yb	0.30	2.73	1.07	1.64	1.50	1.78	1.43	1.59
Lu	0.05	0.45	0.18	0.27	0.24	0.29	0.24	0.26
TOT/C	9.15	5.29	5.23	<0.02	0.02	0.48	0.03	0.14
TOT/S	0.02	<0.02	0.02	<0.02	0.31	<0.02	0.34	0.17
Mo	0.6	0.1	0.38	0.5	0.4	2.6	1.2	1.2
Cu	1.4	4.7	3.53	2.5	10.3	14.3	2.0	7.3
Pb	3.8	8.7	9.67	3.0	355.9	10.2	15.8	96.2
Zn	3	16	17	32	12	53	2	24.8
As	11.8	6.6	10.48	35.9	43.6	0.9	8.6	22.3
Cd	<0.1	0.2	0.12	<0.1	<0.1	<0.1	<0.1	<0.1
Sb	0.2	0.3	0.4	6.0	0.6	<0.1	0.1	1.7
Bi	<0.1	0.2	0.2	0.2	<0.1	<0.1	0.1	<0.1
Ag	<0.1	<0.1	0.1	<0.1	<0.1	<0.1	<0.1	<0.1
Au (ppb)	<0.5	0.5	1.4	<0.5	4.0	0.9	<0.5	<1.5
Hg	0.01	0.02	0.01	<0.01	0.04	<0.01	0.07	<0.03
Tl	0.2	0.3	0.27	<0.1	1.1	<0.1	0.2	<0.4
Se	<0.5	<0.5	0.5	<0.5	2.8	<0.5	<0.5	<1.1
ΣREE	22.0	126.6	65.6	180.0	195.2	186.8	144.4	176.6
ΣLREE	16.4	74.6	46.37	149.6	172.1	150.4	118.3	147.6
ΣMREE	1.9	15.5	6.57	11.4	8.5	13.8	10.7	11.1
ΣHREE	0.7	6.6	2.47	3.8	3.2	4.2	3.2	3.6
Eu/Eu*	0.60	0.48	0.53	0.73	0.58	0.54	1.87	0.93

ΣREE = the sum of (La–Lu)+Y; ΣLREE = the sum of La–Nd; ΣMREE = the sum of (Sm–Ho); ΣHREE = the sum of (Er–Lu); and Eu/Eu* = $Eu_N/\sqrt{(Sm_N*Gd_N)}$ (Mongelli 1997), where N refers to a chondrite-normalized value (Sun & McDonough 1989)

Table 3 Mass gains and losses of major oxides (g) and trace elements (ppm) for the bentonite based on the isocon analysis diagram (Grant 1986, 2005; López-Moro 2012)

			Overall volume change (%)	2.30
			Overall mass change (%)	0.00
			Slope	1.00
Sample	Tuff Avg. (n = 4)	Bentonite Avg. (n = 13)		
Major oxides (wt. %)	Unaltered C^0	Altered C^A	Gain/Loss relative to C_i^0 $\Delta C_i/C_i^0$	Gain/Loss (wt.%) ΔC_i
SiO_2	63.87	55.10	–0.14	–8.77
TiO_2	0.53	0.21	–0.60	–0.32
Al_2O_3	15.57	14.77	–0.05	–0.80
Fe_2O_3	2.83	2.30	–0.19	–0.53
MnO	0.06	0.06	0.00	0.00
MgO	2.44	4.40	0.80	1.96
CaO	2.10	2.30	0.10	0.20
Na_2O	1.78	0.49	–0.72	–1.29
K_2O	3.61	1.48	–0.59	–2.13
P_2O_5	0.10	0.04	–0.60	–0.06
Trace elements (ppm)				Gain/Loss (ppm)
As	22.30	19.01	–0.15	–3.29
Cs	8.00	37.88	3.74	29.88
Rb	123.10	103.32	–0.16	–19.78
Ba	883.00	294.92	–0.67	–588.08
Sr	267.60	126.32	–0.53	–141.28
Pb	96.20	37.86	–0.61	–58.34
Cr	20.53	34.21	0.67	13.68
Ni	3.40	13.43	2.95	10.03
V	77.80	34.08	–0.56	–43.72
Ga	15.40	16.02	0.04	0.62
Zn	24.80	26.69	0.08	1.89
Bi	0.10	0.55	4.50	0.45
U	6.70	3.03	–0.55	–3.67
Zr	171.10	114.40	–0.33	–56.70
Hf	4.70	4.28	–0.09	–0.42
Y	14.30	24.83	0.74	10.53
Nb	11.50	19.07	0.66	7.57
Ta	1.10	1.72	0.56	0.62
Th	24.00	32.92	0.37	8.92
Tl	0.40	0.93	1.33	0.53
La	43.10	31.66	–0.27	–11.44
Ce	72.60	58.98	–0.19	–13.62
Pr	7.24	6.39	–0.12	–0.85
Nd	24.70	22.42	–0.09	–2.28
Sm	3.88	4.72	0.22	0.84
Eu	0.90	0.51	–0.43	–0.39
Gd	2.98	4.13	0.39	1.15
Tb	0.42	0.68	0.62	0.26
Dy	2.41	4.12	0.71	1.71
Ho	0.50	0.84	0.68	0.34
Er	1.52	2.50	0.64	0.98
Tm	0.23	0.38	0.65	0.15
Yb	1.59	2.62	0.65	1.03
Lu	0.26	0.41	0.58	0.15

https://doi.org/10.1007/s42860-019-00029-w Published online by Cambridge University Press

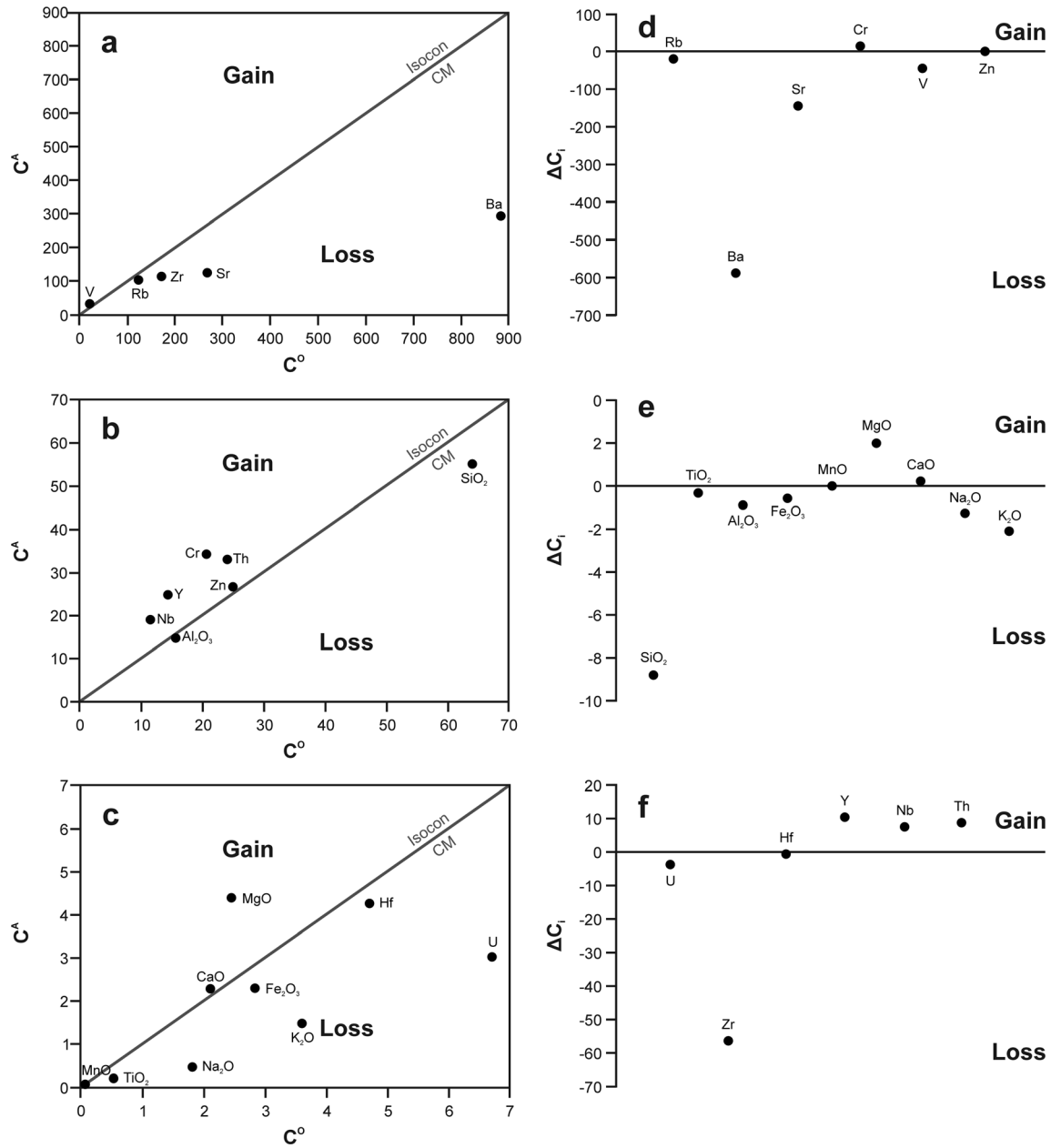

Fig. 9 Mass changes **(a-f)** in the major element (g) and trace element (ppm) contents within the study area based on the isocon analysis diagram (Grant 1986, 2005; López-Moro 2012)

characteristics, although in general they tend to have more basic affinities compared with their counterparts in the present study.

Smectite Chemistry

The structural formulae for the smectites of samples CLD-4, CLD-11, CGS-18, and BRK-6, calculated from the chemical analysis of clay fractions, are typical of montmorillonite (Table 4) with an average estimated structural formula of

$$(Ca_{0.31}Na_{0.05}K_{0.08})(Al_{2.72}Fe_{0.17}Mg_{1.27}Ti_{0.011}Mn_{0.01})(Si_{7.94}Al_{0.06})O_{20}(OH)_4$$

The smectite is Fe-poor, indicating that the parent rocks might be of acidic composition (Christidis 2008) in accordance with the projection in the discrimination diagrams (Figs 11 and 12). The $Na^+/(Na^+ + Ca^{2+})$ ratios suggest Ca-rich bentonite, in accordance with the XRD traces of the bulk samples and the air-dried oriented clay fractions, which show smectite d_{001}

https://doi.org/10.1007/s42860-019-00029-w Published online by Cambridge University Press

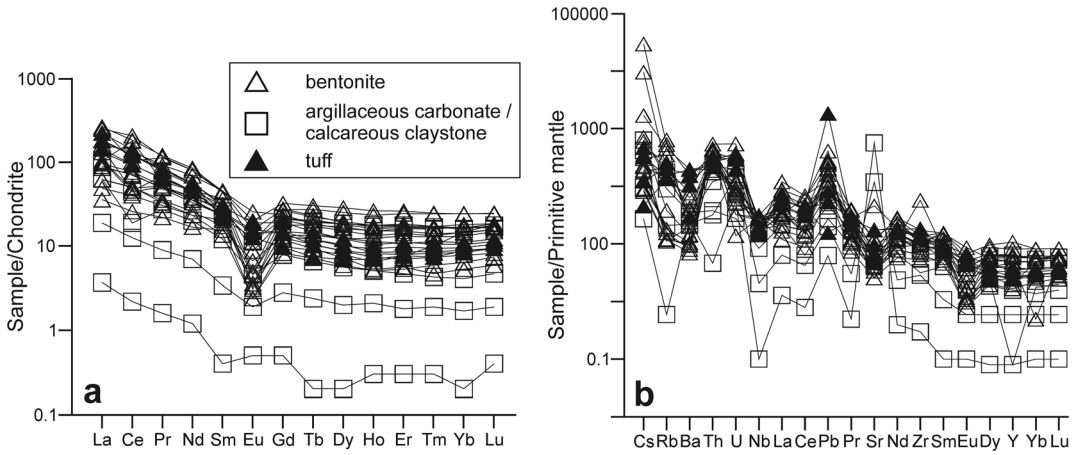

Fig. 10 Chondrite- and primitive mantle-normalized patterns for Balıkesir bentonite and volcanic samples (Sun & McDonough 1989)

spacings typical of smectites with bivalent exchangeable cations (Fig. 6). Moreover, the octahedral occupancy is considerably larger than 4 (Table 4, see also average smectite structural formula), indicating that some of the Mg might also be present in the interlayer.

DISCUSSION

Alteration Patterns in Bentonite Formation

The bentonite deposits in the Çaldere, Yeniköy, Çağış, and Bereketli areas in the Balıkesir region, Turkey, consist of alternating claystone and mudstone associated with limestone, and developed by diagenetic processes in the Miocene Bigadiç volcano-sedimentary units which were deposited in local tectonically controlled depression zones (Fig. 13). The Bigadiç volcano-sedimentary units, which hosted and intercalated bentonite and borate deposits, are composed of rhyolitic and andesitic Sındırgı volcanics, Gölcük basalt, trachyandesitic dikes of the Kayırlar volcanics, and basaltic-andesitic Şahinkaya volcanics. The Çaldere and Çağış bentonites were derived from acidic rocks, whereas their counterparts of the Yeniköy and Bereketli deposits display more basic (andesitic-trachyandesitic) affinities (Fig. 11). The bentonites from the eastern Aegean and Thrace of Upper Oligocene–Upper Miocene age (Koutsopoulou et al. 2016) are plotted in the same diagram. Except for the Samian bentonites, which have alkaline (trachytic) affinities, the remaining eastern Aegean and Thracean bentonites were derived from volcanic rocks of more basic affinities than their counterparts of this study. Smectite abundant claystone beds enclosing desiccation cracks, plant rootlets, and locally Fe-(oxyhydr)oxide stains are in close contact with volcanic materials of the basin and continued with an ostracod- and foraminifera-bearing carbonate, alternating with marl, claystone, and sandstone in an upward sequence. About 50 km to the south (outside the study area) bituminous shale and coal levels are also enclosed (Akyürek & Akdeniz 1989), suggesting a lacustrine–palustrine sedimentation environment.

Smectite is abundant and detrital materials (such as chlorite and rock fragments) are absent from the Balıkesir bentonite deposits that are interbedded or overlain by carbonate rocks. This suggests that the bentonite deposits formed authigenically as 'primary bentonites' from volcanoclastic materials deposited in a calm lacustrine–palustrine environment during the early

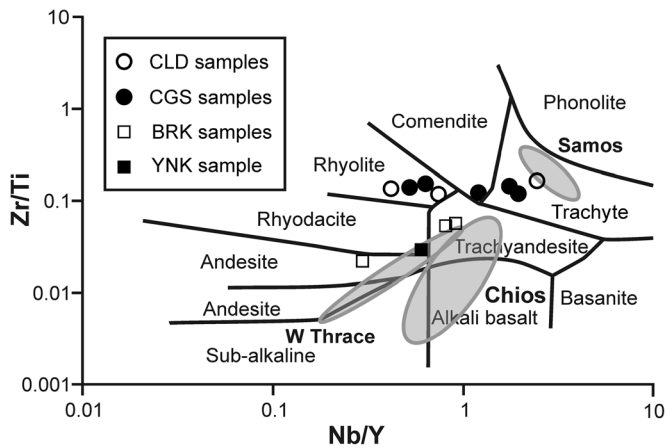

Fig. 11 Geochemical discrimination plot of the bentonite and parent volcanic samples using immobile elements Nb/Y vs. Zr/Ti diagram (Winchester & Floyd 1977) and comparison with the bentonites from the eastern Aegean and Thrace (data from Koutsopoulou et al. 2016)

https://doi.org/10.1007/s42860-019-00029-w Published online by Cambridge University Press

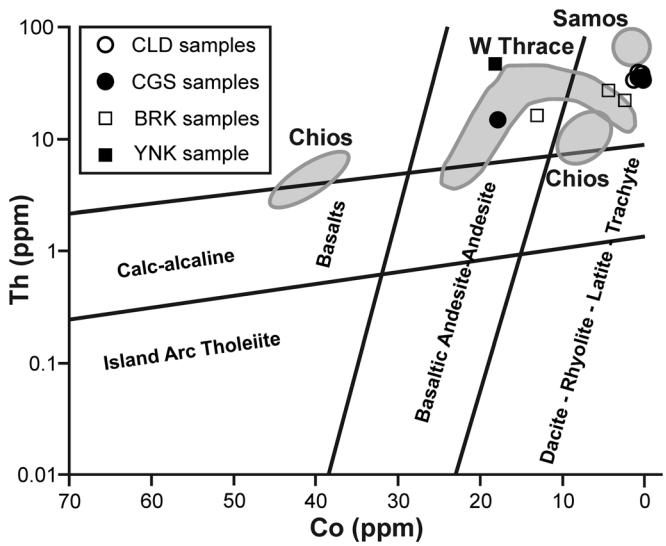

Fig. 12 Geochemical discrimination plot of Balıkesir bentonite using crossplot of Co vs. Th (Hastie et al. 2007), and comparison with the bentonites from the eastern Aegean and Thrace (data from Koutsopoulou et al. 2016)

diagenesis by dissolution-precipitation reactions similar to those underlined by Jeans et al. (1982), Takagi et al. (2005), and Kadir et al. (2017). Thus, volcanic glass shards along with feldspar, biotite, and hornblende crystals were subjected to early diagenetic processes after deposition and were converted to primary bentonite (Fig. 13).

The development of sericitization in feldspar, partial formation of Fe-(oxyhydr)oxides, and chloritization of hornblende and biotite in rhyolitic and andesitic tuff, plus formation of smectite in microfractures and dissolution voids of altered feldspar and mica, suggest a dissolution and precipitation mechanism. Locally, abundant euhedral dolomite crystals in dissolution voids of volcanic units suggest that the sedimentary environment was subjected to alternation of wet and dry periods during early diagenesis (Wright & Tucker 1991). The association of calcified filament structures with dolomite and smectite attests to the presence of biological activity during diagenetic processes (c.f. Wright 1986; Eren et al. 2018).

The significant depletion of SiO_2, Ba, Sr, Pb, V, and Zr, but less of K_2O, Fe_2O_3, Na_2O, and Rb, and the enrichment of MgO and CaO, during alteration of glass shards and volcanogenic minerals favored formation of smectite under alkaline conditions and an open hydraulic system (Fig. 9; Dible & Tiller 1981; Christidis & Scott 1997). In contrast MnO, Al_2O_3, and TiO_2 are virtually immobile, similar to the findings of previous studies (Zielinski 1982; Christidis 1998). In addition, the white color of the bentonites suggests Fe- and Ti-poor parent materials, indicating the presence of rhyolitic precursors as was also suggested by discrimination diagrams (Fig. 10), in accordance with previous work (Esenli 1993; Christidis & Scott 1997). The Na and K released might have resulted in local precipitation of heulandite-clinoptilolite in altered volcanic units in Kargın, 30 km southeast of Balıkesir and outside the area studied (Christidis et al. 1995; Ekinci Şans et al. 2015). In the carbonate-rich horizons, calcite and dolomite might have formed by direct chemical precipitation or/and by dolomitization of earlier precipitated calcite during diagenesis.

The Si released during the alteration process resulted in secondary silicification (precipitation of quartz, opal-CT) in the uppermost levels of the bentonite deposit, similar to previous studies (Lavery, 1985; Christidis et al. 1995; Inoue 1995; Kirov et al. 2011; Çiflikli et al. 2013; Malek-Mahmoodi et al. 2013). The high values of Ba (up to 1419 ppm), Sr (1003 ppm), and Zr (132.3 ppm) also support the suggestion of a volcanogenic origin. The K released may also have resulted in the formation of accessory illite. The increases in LREE/(MREE+HREE) and a negative Eu anomaly in the bentonite samples suggest that the Al, Mg, Fe, and Si required for the formation of smectite originated from the alteration of feldspars and volcanic glass during diagenesis (Kadir et al. 2017).

An interesting feature of the alteration of tuffs to bentonite in the study area is the decrease in LREE and Eu contents and the increase in HREE contents during alteration (Tables 2, 3). This trend is the opposite of the observed behavior of REE during alteration of an acidic precursor to bentonite in Kimolos Island, Greece, (Christidis 1998) and is attributed to the minerals hosting REE in the various areas. The Kimolian bentonites and respective parent rocks contain igneous phosphates (apatite and monazite), which host the LREE (Christidis 1998). In contrast, the HREE are present in the original volcanic glass and are leached during alteration. In the present study the bentonites contain very small amounts of P_2O_5 compared with the parent tuffs, suggesting significant P_2O_5 leaching. Therefore, P might not just be associated with phosphate minerals but might also be hosted in the glass, from where it was released during alteration. In contrast, the HREE might be associated, in the rocks studied, with hornblende or biotite, which are largely preserved during alteration (Table 1). Finally, the migration of Eu during alteration (Table 2) is compatible with the alteration of feldspars during alteration as previously mentioned.

https://doi.org/10.1007/s42860-019-00029-w Published online by Cambridge University Press

Table 4 Chemical compositions and structural formulae for purified smectite samples. Calculated based on $O_{20}(OH)_4$

Major oxide (wt.%)	CLD-4 Smectite	CLD-11 Smectite	CGS-18 Smectite	BRK-6 Smectite	Avg. Smectite
SiO_2	50.54	50.7	52.02	52.57	51.46
Al_2O_3	15.23	15.01	15.2	15.75	15.30
Fe_2O_3	1.49	1.69	1.48	1.25	1.48
MgO	5.85	6.6	5.53	4.13	5.53
CaO	1.33	2.0	1.85	2.62	1.95
Na_2O	0.11	0.05	0.09	0.44	0.17
K_2O	0.24	0.32	0.2	0.86	0.40
TiO_2	0.07	0.1	0.08	0.14	0.10
MnO	0.01	0.02	0.04	0.19	0.06
SiO_2/Al_2O_3	3.3	3.3	3.4	3.3	3.3
Tetrahedral					
Si	7.93	7.84	7.99	7.99	7.94
Al	0.07	0.16	0.01	0.01	0.06
Σ	8.00	8.00	8.00	8.00	8.00
Octahedral					
Al	2.75	2.58	2.74	2.81	2.72
Fe	0.17	0.20	0.17	0.14	0.17
Mg	1.37	1.52	1.27	0.93	1.27
Ti	0.008	0.008	0.009	0.02	0.011
Mn	0.001	0.001	0.007	0.03	0.01
Σ	4.30	4.30	4.19	3.93	4.18
Interlayer					
Ca	0.22	0.33	0.30	0.41	0.31
Na	0.03	0.01	0.03	0.13	0.05
K	0.05	0.06	0.04	0.17	0.08
Σ	0.3	0.74	0.37	0.71	0.53
$Na^+/(Na^+ + Ca^{+2})$	0.12	0.03	0.09	0.24	0.12
Tetrahedral charge	0.06	0.15	0.0001	0.01	0.05
Octahedral charge	0.46	0.60	0.67	1.14	0.72
Total charge	0.52	0.76	0.67	1.14	0.77
Interlayer charge	0.51	0.74	0.67	1.13	0.76

Comparison with the eastern Aegean and the Thracean Bentonites

Bentonite deposits are widespread in the broader area of the eastern Aegean, Thrace, and western Anatolia. These deposits bear several similarities and different features in terms of age, geodynamic and geological environment, and parent-rock composition. The age of the bentonites varies from Upper Eocene to Oligocene in Thrace to Upper Miocene in Samos (Ekinci Şans et al. 2015; Koutsopoulou et al. 2016). The depositional environment of the parent rocks varies from being shallow marine-brackish in Thrace to lacustrine in the eastern Aegean (Samos and Chios Islands) and western Anatolia (including the present study), whereas their geochemical affinities vary from calc-alkaline to shoshonitic (Pe-Piper & Piper 2006, 2007; Ekinci Şans et al. 2015; Koutsopoulou et al. 2016). The shoshonitic affinities of the Balıkesir bentonites were suggested by discrimination plots (Fig. 11) and have been shown in previous studies (Koutsopoulou et al. 2016).

An interesting similarity between the eastern Aegean and Balıkesir bentonites formed in lacustrine–palustrine environments from acidic precursors is the type of the parent rock and the spatial development of alteration to bentonite. In the Samos bentonite, the parent rock was an ignimbrite and the bentonite was formed by low-temperature hydrothermal fluids controlled by fault lines (Koutsopoulou et al. 2016). In Chios, the bentonite was formed at the expense of an ash flow, but the alteration to bentonite was not complete because volcanic activity was limited to a single event (Koutsopoulou et al. 2016). In Balıkesir, the parent rocks were airborne tuffs deposited with clastic and carbonate sediments in the lacustrine–palustrine basin. The thickness of the bentonite outcrops, their lateral extent, and their texture are also compatible with

https://doi.org/10.1007/s42860-019-00029-w Published online by Cambridge University Press

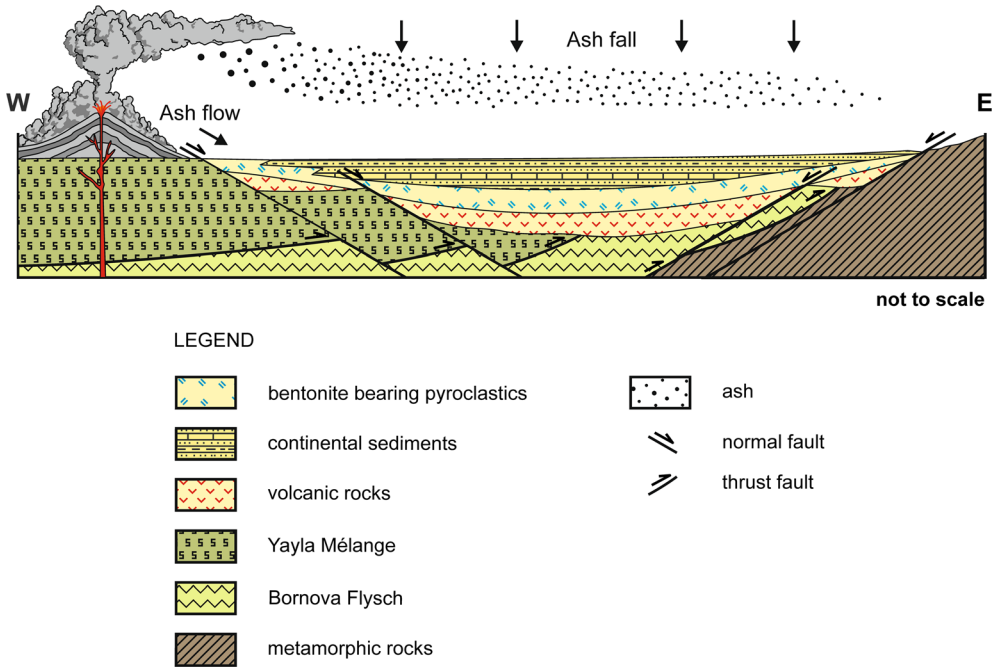

Fig. 13 Sketch of genetic model for the Balıkesir bentonite deposits

slightly welded airborne tuffs characterized by massive feature (Figs. 3 and 4) similar to those reported by Erkül et al. (2005b). The comparable compositions of the parent rocks notwithstanding, the Balıkesir bentonites are richer in smectite than their Samian and Chios counterparts and, in particular, they do not contain abundant opal-CT (Table 1). This suggest that excess Si migrated during alteration of the acidic precursors as was indicated by the mass-balance calculations and the isocon plots (Table 3, Fig. 9). The migration of Si is related to the diagenetic alteration of the tuffs and is associated with fluid flow.

Hence, the question is transferred to the mechanism which facilitated fluid flow in the Balıkesir bentonites compared to their Samian and Chios counterparts. In Samos, the parent ignimbrite behaved like a "geoautoclave" (Aleksiev & Djourova 1975; de'Genarro et al. 2000; Machiels et al. 2014) and alteration to bentonite occurred along fault lines in which the system was open. In Chios, the quick cooling of the parent ash flow caused fast dissipation of heat and partial conversion to bentonite (Koutsopoulou et al. 2016). The field relationships and the textural features of Balıkesir bentonites indicate that the parent rocks were airborne tuffs or slightly welded ash flows and that heat-driven flow might not have been prevalent during alteration. The fluid flow, therefore, may have been related to the development of hydraulic head during diagenesis associated with Neogene tectonics in the broader area.

CONCLUSIONS

The Balıkesir bentonite deposits in western Anatolia formed by a diagenetic process in the Miocene volcano-sedimentary units which were deposited in depression zones. The lithology, mineralogy, and geochemistry of the bentonites containing desiccation cracks, plant rootlets, locally Fe-(oxyhydr)oxide stains, and accompanied by carbonates suggest formation under alternating wet and dry periodic climatic changes in a shallow lacustrine–palustrine environment. Alteration of feldspar, amphibole, and biotite released Al, Mg, and Fe for the formation of smectite under mild alkaline conditions controlled by an open hydraulic system. The high LREE/(MREE+HREE) ratios and negative Eu anomalies suggest that smectite formed diagenetically from volcanic materials.

ACKNOWLEDGMENTS

This study was funded by the Scientific Research Projects of Eskişehir Osmangazi University (Project 2016–1358). The authors are much indebted to Professor Emilia García Romero and an anonymous reviewer for their extremely careful and constructive reviews that improved the quality of the paper significantly. The authors are also very grateful to the anonymous Associate Editor and to the Editor-in-Chief, Joseph W. Stucki for their insightful editorial comments and suggestions. This paper was presented at the 9th Mid-European Clay Conference, 2018, in Zagreb, Croatia. Nergis Önalgil is thanked for assisting during the field work.

Compliance with Ethical Standards

Conflict of Interest

The authors have no conflict of interest and also approve the publication ethics.

REFERENCES

Akdeniz, N. (1980). Başlamış formasyonu [Başlamış formation]. *Jeoloji Mühendisliği Dergisi, 10*, 39–48 [in Turkish with English abstract].

Akyürek, B. & Akdeniz, N. (1989). Geological Map of Balıkesir G 5 Quadrangle, Scale 1:100.000, *General Directorate of Mineral Research and Exploration (MTA) Publications*, Ankara, Turkey.

Aleksiev, B. & Djourova, E. G. (1975). On the origin of zeolite rocks. *Comptes Rendus de l'Académie Bulgare de Sciences, 28*, 517–520.

Bakır, S., Akbulut, A., Kapkaç, F., Karahan, D.S., & Çetin C. (2012). Türkiye Bentonit Envanteri (Envanter Serisi 204), Maden Tetkik ve Arama Genel Müdürlüğü, Ankara [Turkey Bentonite Inventory (Inventory Series 204), Ankara, Turkey, General Directorate of Mineral Research and Exploration].

Christidis, G. & Dunham, A. C. (1997). Compositional variations in smectites. Part II: Alteration of acidic precursors. A case study from Milos Island, Greece. *Clay Minerals, 32*, 253–270.

Christidis, G. & Scott, P. W. (1997). The origin and control of colour of white bentonites from the Aegean islands of Milos and Kimolos, Greece. *Mineralium Deposita, 32*, 271–279.

Christidis, G., Scott, P. W., & Marcopoulos, T. (1995). Origin of the bentonite deposits of Eastern Milos and Kimolos, Greece: geological, mineralogical and geochemical evidence. *Clays and Clay Minerals, 43*, 63–77.

Christidis, G. E. (1998). Comparative study of the mobility of major and trace elements during alteration of an andesite and a rhyolite to bentonite, in the islands of Milos and Kimolos, Aegean, Greece. *Clays and Clay Minerals, 46*, 379–399.

Christidis, G. E. (2001). Formation and growth of smectites in bentonites: A case study from Kimolos Island, Aegean, Greece. *Clays and Clay Minerals, 49*, 204–215.

Christidis, G. E. (2008). Do bentonites have contradictory characteristics? An attempt to answer unanswered questions. *Clay Minerals, 43*, 515–529.

Çiflikli, M., Çiftçi, E., & Bayhan, H. (2013). Alteration of glassy volcanic rocks to Naand Ca-smectites in the Neogene basin of Manisa, western Anatolia, Turkey. *Clay Minerals, 48*, 513–527.

Çoban, F. (2014). Bigadiç (Balıkesir) Bentonit Yataklarının Mineralojisive Jeokimyası ve bentonitleşme sırasındaki ana, eser ve nadir toprak elementlerinin mobilizasyonu. *Çukurova University Journal of the Faculty of Engineering and Architecture, 29*, 55–68 [in Turkish with English abstract].

de'Genarro, M., Cappelletti, P., Langella, A., Perrotta, A., & Scarpati, C. (2000). Genesis of zeolites in the Neapolitan Yellow Tuff: geological, volcanological and mineralogical evidence. *Contributions to Mineralogy and Petrology, 139*, 17–35.

Dible, W. E., Jr., & Tiller, W. A. (1981). Kinetic model of zeolite paragenesis in tuffaceous sediments. *Clays and Clay Minerals, 29*, 323–330.

Ece, O. I., & Schroeder, P. A. (2007). Clay mineralogy and chemistry of halloysite and alunite deposits in the Turplu area, Balikesir, Turkey. *Clays and Clay Minerals, 55*, 18–35.

Ece, Ö. I., Schroeder, P. A., Smilley, M. J., & Wampler, J. M. (2008). Acid-sulfate alteration volcanic rocks and genesis of halloysite and alunite deposits in the Biga Peninsula, NW Turkey. *Clay Minerals, 43*, 281–315.

Ece, Ö. İ., Ekinci, B., Schroeder, P. A., Crowe, D., & Esenli, F. (2013). Origin of the Düvertepe kaolin-alunite deposits in Simav Graben, Turkey: Timing and Styles of hydrothermal mineralization. *Journal of Volcanology and Geothermal Research, 255*, 57–18.

Ekinci Şans, B., Esenli, F., Kadir, S., & Elliott, W. C. (2015). Genesis of smectite in siliciclastics and pyroclastics of the Eocene İslambeyli Formation in the Lalapaşa region, NW Thrace, Turkey. *Clay Minerals, 50*, 459–483.

Elliott, W. C. (1993). Origin of the Mg smectite at the Cretaceous/Tertiary (K/T) boundary at Stevns Klint, Denmark. *Clays and Clay Minerals, 41*, 442–452.

Erdoğan, B., Altıner, D., Güngör, T., & Özer, S. (1990). Stratigraphy of Karaburun peninsula. *Maden Tetkik ve Arama Dergisi*, 111, 1–23.

Eren, M., Yeşilot Kaplan, M., Kadir, S., & Kapur, S. (2018). Biogenic (β-fabric) features in the hard laminated crusts of the Mersin and Adana regions, southern Turkey and their role in calcrete development. *Catena, 168*, 34–46.

Erkül, F., Helvacı, C., & Sözbilir, H. (2005a). Evidence for two episodes of volcanism in the Bigadiç borate basin and tectonic implications for western Turkey. *Geological Journal, 40*, 545–570.

Erkül, F., Helvacı, C., & Sözbilir, H. (2005b). Stratigraphy and Geochronology of the Early Miocene Volcanic Units in the Bigadiç Borate Basin, Western Turkey. *Turkish Journal of Earth Sciences, 14*, 227–253.

Esenli, F. (1993). The chemical changes during zeolitization (heulandite-clinoptilolite type) of the acidic tuffs in the Gördes Neogene basin. *Geological Bulletin of Turkey, 36*, 37–44 [in Turkish with English abstract].

Ghanem, H., & Jarrar, G. H. (2013). Geochemistry and petrogenesis of the 595 Ma shoshonitic Qunai monzogabbro, Jordan. *Journal of African Earth Sciences, 88*, 1–14.

Grant, J. A. (1986). The isocon diagram – a simple solution to Gresens' equation for metasomatic alteration. *Economic Geology, 81*, 1976–1982.

Grant, J. A. (2005). Isocon analysis: A brief review of the method and applications. *Physics and Chemistry of the Earth, 30*, 997–1004.

Grim, R. E., & Güven, N. (1978). *Bentonites, Geology, Mineralogy, Properties and Uses* (pp. 13–137). Amsterdam: Elsevier.

Harnois, L. (1988). The CIW index: a new Chemical Index of Weathering. *Sedimentary Geology, 55*, 319–322.

Hastie, A. R., Kerr, A. C., Pearce, J. A., & Mitchell, S. F. (2007). Classification of altered Volcanic Island Arc Rocks using immobile trace elements: development of the Th-Co discrimination diagram. *Journal of Petrology, 48*, 2341–2357.

Huff, W. D. (2016). K-bentonites: A review. *American Mineralogist, 101*, 43–70.

Huff, W. D., Anderson, T. B., Rundle, C. C., & Odin, G. S. (1991). Chemostratigraphy, K-Ar ages and illitization of Silurian K-bentonites from the Central Belt of the Southern Uplands-Down-Longford terrane, British Isles. *Journal of the Geological Society, 148*, 861–868.

Inoue, A. (1995). Formation of Clay Minerals in Hydrothermal Environments. In B. Velde (Ed.), *Origin and Mineralogy of Clays, Clays and the Environment* (pp. 268–329). Berlin: Springer-Verlag.

Jeans, C. V., Merriman, R. J., Mitchell, J. G., & Bland, D. J. (1982). Volcanic clays in the Cretaceous of southern England and northern Ireland. *Clay Minerals, 17*, 105–156.

Kadir, S. & Akbulut, A. (2009). Mineralogy, geochemistry and genesis of the Taşoluk kaolinite deposits in pre-Early Cambrian metamorphites and Neogene volcanites of Afyonkarahisar, Turkey. *Clay Minerals, 44*, 89–112.

Kadir, S., Erman, H., & Erkoyun, H. (2011). Mineralogical and geochemical characteristics and genesis of hydrothermal kaolinite deposits within Neogene volcanites, Kütahya (western Anatolia), Turkey. *Clays and Clay Minerals, 59*, 250–276.

Kadir, S. & Kart, F. (2009). Occurrence and origin of the Söğüt kaolinite deposits in the Paleozoic Saricakaya granite–granodiorite complexes and overlying Neogene sediments (Bilecik, northwestern Turkey). *Clays and Clay Minerals, 57*, 311–329.

Kadir, S., Külah, T., Önalgil, N., Erkoyun, H., & Elliott, W. C. (2017). Mineralogy, geochemistry, and genesis of bentonites in Miocene volcanic-sedimentary units of the Ankara-Çankırı Basin, central Anatolia, Turkey. *Clays and Clay Minerals, 65*, 64–92.

Kirov, G., Šamajova, E., Nedialkov, R., & Stanimirova, T. S. (2011). Alteration processes and products of acid pyroclastic rocks in Bulgaria and Slovakia. *Clay Minerals, 46*, 279–294.

Kocabaş, C. (2006). *Yeniköy (Bigadiç) Doğusundaki Bentonit Oluşumlarının Mineralojik-Jeokimyasal İncelemesi*. M.Sc. Thesis, Balıkesir University, Turkey, pp. 92 [in Turkish with English abstract].

Konuk, T. (1977). Bornova filişinin yaşı hakkında [On the age of Bornova flysch]. *Ege Üniversitesi Fen Fakültesi Dergisi, B1*, 65–74 [in Turkish with English abstract].

Koutsopoulou, E., Christidis, G. E., & Marantos, I. (2016). Mineralogy, geochemistry and physical properties of bentonites from the western Thrace Region and the islands of Samos and Chios, east Aegean, Greece. *Clay Minerals, 51*, 563–588.

Kunze, G.W., & Dixon, J.B. (1986). Pretreatment for mineralogical analysis. In A. Klute (Ed.), *Methods of Soil Analysis, Part 1. Physical and Mineralogical Methods* (2nd edition) (pp. 91–100). American Society of Agronomy, Inc. and the Soil Science Society of America, Inc., Madison, Wisconsin, USA.

Lavery, N. G. (1985). Quantifying chemical changes in hydrothermally altered volcanic sequences – silica enrichment as a guide to the Crandon massive sulfide deposit, Wisconsin, U.S.A. *Journal of Geochemical Exploration, 24*, 1–27.

López-Moro, F. J. (2012). EASYGRESGRANT – A Microsoft Excel spreadsheet to quantify volume changes and to perform mass-balance modeling in metasomatic systems. *Computers and Geosciences, 39*, 191–196.

Machiels, L., Garcés, D., Snellings, R., Vilema, W., Morante, F., Paredes, C., & Elsen, J. (2014). Zeolite occurrence and genesis in the Late-Cretaceous Cayo arc of Coastal Ecuador: Evidence for zeolite formation in cooling marine pyroclastic flow deposits. *Applied Clay Science, 87*, 108–119.

Malek-Mahmoodi, F., Khalili, M., & Mirlohi, A. (2013). The origin of the bentonite deposits of Tashtab Mountains (Central Iran): Geological, Geochemical, and Stable Isotope evidences. *Geopersia, 3*, 73–86.

Mongelli, G. (1997). Ce-anomalies in the textural components of Upper Cretaceous karst bauxites from the Apulian carbonate platform (southern Italy). *Chemical Geology, 140*, 69–79.

Motoki, A., Sichel, S. E., Vargas, T., Melo, D. P., & Motoki, K. F. (2015). Geochemical behaviour of trace elements during fractional crystallization and crustal assimilation of the felsic alkaline magmas of the state of Rio de Janeiro, Brazil. *Anais da Academia Brasileira de Ciências (Annals of the Brazilian Academy of Sciences), 87*, 1959–1979.

MTA (2002). 1/500,000 scale geological map of Turkey – İzmir, General Directorate of Mineral Research and Exploration of Turkey.

Mutlu, H., Sarıız, K., & Kadir, S. (2005). Geochemistry and origin of the Şaphane alunite deposit, Western Anatolia, Turkey. *Ore Geology Reviews, 26*, 39–50.

Okay, A.İ., Satır, M., Siyako, M., Monie, P., Metzger, R., & Akyüz, S. (1996). Paleo- and Neo-Tethyan events in northwestern Turkey: geologic and geochronological constrains. In A. Yin & T.M. Harrison (Eds.), *The Tectonic Evolution of Asia* (pp. 420–441). Cambridge University Press, Cambridge, UK.

Okay, A. İ., & Siyako, M. (1993). The revised location of the İzmir-Ankara Suture in the region between Balıkesir and İzmir. In S. Turgut (Ed.), *Tectonics and Hydrocarbon Potential of Anatolia and Surrounding Regions* (pp. 333–355). Ankara: Ozan Sungurlu Symposium Proceedings.

Okay, A. İ., Tansel, İ., & Tüysüz, O. (2001). Obduction, subduction and collision as reflected in the Upper Cretaceous-Lower Eocene sedimentary record of western Turkey. *Geological Magazine, 138*, 117–142.

Osborn, S. G., Duffield, L. T., Elliott, W. C., Wampler, J. M., Elmore, R. D., & Engel, M. H. (2014). The timing of diagenesis and thermal maturation of the Cretaceous Marias River Shale, Disturbed Belt, Montana. *Clays and Clay Minerals, 62*, 112–125.

Paz, S. P. A., Angélica, R. S., & Neves, R. F. (2012). Mg-bentonite in the Parnaíba Paleozoic Basin, Northern Brazil. *Clays and Clay Minerals, 60*, 265–277.

Pehlivan, Ş., Duru, M., Dönmez, M., Ilgar, A., Akçay, E., Erdoğan, K., & Özer, D. (2007). Geological Map of Bandırma H 19 Quadrangle, Scale 1:100.000, *General Directorate of Mineral Research and Exploration (MTA) Publications*, Ankara, Turkey.

Pe-Piper, G., & Piper, D. J. W. (2006). Unique features of the Cenozoic igneous rocks of Greece. In Y. Dilek & S. Pavlides (Eds.), *Postcollisional tectonics and magmatism in the Mediterranean Region and Asia* (pp. 259–282). Geological Society of America Special Paper 409.

Pe-Piper G. & Piper, D.J.W. (2007). New insights into the relationship between magmatism and tectonics. In L. Beccaluva, G. Bianchini & M. Wilson (Eds.), *Cenozoic Volcanism in the Mediterranean Area* (pp. 17–31). Geological Society of America Special Paper 417.

Ray, D. C., Collings, A. J. V., Worton, G. J., & Jones, G. (2011). Upper Wenlock bentonites from Wren's Nest Hill, Dudley: comparisons with prominent bentonites along Wenlock Edge, Shropshire, England. *Geological Magazine, Cambridge University Press, 148*, 670–681.

Środoń, J., Clauer, N., Banas, M., & Wójtowicz, A. (2006). K-Ar evidence for a Mesozoic thermal event superimposed on burial diagenesis of the Upper Silesia Coal Basin. *Clay Minerals, 41*, 669–690.

Sun, S.-s., & McDonough, W. F. (1989). *Chemical and isotopic systematics of oceanic basalts: implications for mantle composition and processes*. London, UK: Geological Society.

Takagi, T., Koh, S. M., Song, M. S., Itoh, M., & Mogi, K. (2005). Geology and properties of the Kawasaki and Dobuyama bentonite deposits of Zao region in northeastern Japan. *Clay Minerals, 40*, 333–350.

Ver Straeten, C. A. (2004). K-bentonites, volcanic ash preservation, and implications for Early to Middle Devonian volcanism in the Acadian orogen, eastern North America. *Geological Society of America, 116*, 474–489.

Weaver, C. E. & Beck, K. (1977). Miocene of the S.E. United States: A Model for chemical sedimentation in a peri-marine environment. Special Issue. *Sedimentary Geology, 17*, 1–234.

Whitney, D. L. & Evans, B. W. (2010). Abbreviations for names of rock-forming minerals. *American Mineralogist, 95*, 185–187.

Winchester, J. A. & Floyd, P. A. (1977). Geochemical discrimination of different magma series and their differentiation products using immobile elements. *Chemical Geology, 20*, 245–252.

Wright, V. P. (1986). The role of fungal biomineralization in the formation of early Carboniferous soil fabrics. *Sedimentology, 33*, 831–838.

Wright, V. P., & Tucker, M. E. (1991). *Calcretes*. Oxford: Blackwell Scientific Publications 351 pp.

Wulaningsih, T., Humaida, H., Harijoko, A., & Watanabe, K. (2013). Major element and rare earth elements investigation of Merapi volcano, central Java, Indonesia. *Procedia Earth and Planetary Science, 6*, 202–211.

Zielinski, R. A. (1982). The mobility of uranium and other elements during alteration of rhyolite ash to montmorillonite: A case study in the troublesome formation, Colorado, USA. *Chemical Geology, 35*, 185–204.